## Geophysical Journal International

Royal Astronomical Society

Geophys. J. Int. (2024) 239, 218–235 Advance Access publication 2024 August 09 GJI Geomagnetism and Electromagnetism https://doi.org/10.1093/gji/ggae268

# Thermal rock magnetic cycling (TRMC): a method to track thermal alteration details for palaeointensity interpretations

Junxiang Miao <sup>1,2</sup> and Huapei Wang <sup>2</sup>

Accepted 2024 July 26. Received 2024 July 13; in original form 2024 February 29

### SUMMARY

Accurate absolute palaeointensity is essential for understanding dynamo processes on the Earth and other planetary bodies. Although great efforts have been made to propose techniques to obtain magnetic field strength from rock samples, such as Thellier-series methods, the amount of high-fidelity palaeointensities remains limited. One primary reason for this is the thermal alteration of samples that pervasively occurred during palaeointensity experiments. In this study, we developed a comprehensive rock magnetic experiment, termed thermal rock magnetic cycling (TRMC), that can utilize measurements of critical rock magnetic properties at elevated temperatures during multiple heating-cooling cycles to track thermal changes in bulk samples and individual magnetic components with different Curie temperatures in samples for palaeointensity interpretations. We demonstrate this method on a Galapagos lava sample, GA 84.6. The results for this specimen revealed that GA 84.6v underwent thermophysical alteration throughout the TRMC experiment, resulting in changes in its remanence carrying capacity. These findings were then used to interpret the palaeointensity results of specimen GA 84.6c, which revealed that the two-slope Arai plot yielded two linear segments with distinct palaeointensity values that were both biased by thermophysical alteration. To further test the TRMC method, we selected another historical lava sample (HS 2) from Mt Lassen, detecting slight thermal-physical changes after heating the specimen HS 2-8C to a target temperature of 400 °C. We also isolated a stable magnetic component with a Curie temperature below 400 °C using the TRMC method, which may provide a more reliable palaeointensity estimate of 51  $\mu$ T. By providing a method for tracking thermal alteration independent of palaeointensity experiments, the TRMC method can explore subtle, unrecognizable thermal alteration processes in less detailed palaeointensity measurements, which can help to assess the thermal stability of the measured samples and interpret the changes in the TRM unblocking spectrum and palaeointensity estimates, facilitating the acquisition of more reliable records for constrain the formation of the inner core and the evolution of Earth's magnetic field.

**Key words:** Magnetic properties; Palaeointensity; Rock and mineral magnetism; Instability analysis.

### 1 INTRODUCTION

One of the central goals of palaeomagnetic research is to describe variations in the geomagnetic field, including its direction and strength. Accurate palaeointensity records play a pivotal role in understanding geomagnetic field behaviour (e.g. de Groot *et al.* 2015; Wang *et al.* 2015; Okayama *et al.* 2019; Asefaw *et al.* 2021) and the evolution of dynamos within the core of the Earth and other planetary bodies (e.g. Biggin *et al.* 2015; Tikoo *et al.* 2017; Bono *et al.* 2019; Mighani *et al.* 2020). Furthermore, insights into the formation and early history of the solar system can be gleaned from

palaeointensity estimates of meteorites (e.g. Fu et al. 2014; Wang et al. 2017; Fu et al. 2020; Weiss et al. 2021).

A significant amount of the absolute palaeointensity records was acquired using the Thellier-series palaeointensity experiments, which used heating treatments to replace natural remanent magnetization (NRM) recorded by measured rock samples with a thermal remanent magnetization (TRM) obtained by a known laboratory-applied field (Thellier & Thellier 1959; Coe 1967b). Widely used Thellier-series method, such as the original Thellier-Thellier double heating protocol (Thellier & Thellier 1959), the Coe protocol (Coe 1967b) and the IZZI protocol (Tauxe & Staudigel 2004; Yu

<sup>&</sup>lt;sup>1</sup>School of Earth Sciences, China University of Geosciences, Wuhan, Hubei 430074, China

<sup>&</sup>lt;sup>2</sup>Palaeomagnetism and Planetary Magnetism Laboratory, School of Geophysics and Geomatics, China University of Geosciences, Wuhan, Hubei 430074, China. E-mail: huapei@cug.edu.cn

et al. 2004), have several challenges for obtaining reliable palaeointensity data, resulting in a low success rate in these protocols and a limitation in the acquisition of available accurate palaeointensities. For example, global palaeointensity records spanning the past 5 Myr drawn from the PINT 2014.01 database did not exhibit an explicit latitudinal dependency as expected for a geocentric axial dipole (GAD) model (e.g. Lawrence et al. 2009; Wang et al. 2015; Biasi et al. 2021; Tauxe et al. 2022). One possible primary reason for this is the low-fidelity palaeointensity data in the database (Wang et al. 2015).

Based on empirical and experimental arguments from previous studies over past decades, the thermal alteration of samples (Kosterov & Prévot 1998; Fabian 2009; Qin et al. 2011; Zhao et al. 2014; Kim et al. 2018; Wang & Kent 2013, 2021) and the multidomain (MD) effect (Levi 1977; Riisager & Riisager 2001; Xu & Dunlop 2004; Biggin 2006; Dunlop 2011; Shaar et al. 2011; Smirnov et al. 2017; Tauxe et al. 2021), are the two crucial reasons restrict the fidelity of palaeointensity determinations during Thellier-type methods. Great efforts have been made, such as low-temperature demagnetization (LTD) treatments (Schmidt 1993; Smirnov et al. 2017) and the Repeat thEllier-Series ExperimenT (RESET) palaeointensity method (Wang & Kent 2021) to correct the MD effect and have gradually improved success rates in palaeointensity experiments (Biggin & Dekkers 2007; Paterson 2011; Smirnov et al. 2017; Wang & Kent 2021).

Thermal alteration of lava samples, including thermophysical (such as variations in magnetic domain state) and thermochemical (such as the formation of new ferromagnetic minerals or the degradation of original ferromagnetic minerals) changes, are commonly occurred in laboratory heating process during Thellier-series palaeointensity experiments, which can bias the palaeointensity estimates (Qin et al. 2011; de Groot et al. 2014; Wang & Kent 2021). The partial thermoremanence check (pTRM check), first proposed by Thellier & Thellier (1959), is conducted by giving the sample another pTRM at a previously experienced lower temperature during palaeointensity measurements to detect possible changes in the magnetic mineralogy. A discrepancy between the previously acquired pTRM and the pTRM obtained during the check process at the same temperature indicates that thermal alteration occurred. In the current studies, pTRM checks as the primary thermal alteration indicator widely used in palaeointensity experiments (Monster et al. 2018; Abdulghafur & Bowles 2019; Grappone et al. 2021; Wang & Kent 2021). For example, 88 per cent of 25 palaeointensity studies collected from 2003 to 2014 used pTRM checks (see table S1 in Wang & Kent 2021). However, the pTRM check has its inherent weakness, which is only effective in detecting thermal changes within particles whose blocking temperature is lower than the check temperature (Coe 1967a; Wang & Kent 2021), resulting in even passing the pTRM check does not guarantee the thermal stability of the measured samples and the accuracy of obtained palaeointensity estimates.

Great effort has been made to propose different palaeointensity experimental techniques to avoid thermal alteration, such as the multispecimen parallel differential pTRM technique (referred to as the MS method, Hoffman *et al.* 1989; Dekkers & Böhnel 2006). The MS method complied with a basic assumption of the first-order symmetry properties of pTRM in MD grains (Dekkers & Böhnel 2006) to obtain reliable palaeointensities independent of magnetic domain states (Dekkers & Böhnel 2006; Michalk *et al.* 2008; 2010). Moreover, the MS method uses multiple samples, and each sample conducted one moderate-temperature heating treatment, avoiding laboratory-induced thermal alterations and reducing the processing

time duration (Dekkers & Böhnel 2006). However, the sample conducted in the once-heating step may not avoid thermal alteration, and the MS method still needs the rock magnetic measurements to identify the thermal stability of measured samples.

Conventional measurements of rock magnetic properties before and after heating steps serve as another indicator to detect thermal changes (Smirnov & Tarduno 2003; Carvallo *et al.* 2006; Qin *et al.* 2011; Paterson *et al.* 2017; Kim *et al.* 2018; Wang & Kent 2021). For instance, Qin *et al.* (2011) identified the  $M_{\rm rs,480^{\circ}C}/M_{\rm rs,25^{\circ}C}$  as the alteration index to select palaeointensity samples without thermal changes. Jeong *et al.* (2021) compared hysteresis properties before and after heating treatments to detect the possible thermal changes to recover the geomagnetic field intensities from the Hawaii 1960 historical lava samples. Paterson *et al.* (2017) established a link between magnetic behaviour and palaeointensity estimates and identified the bulk domain stability (BDS) trend to reveal the remanence stability of measured samples. These findings show that comprehensive rock magnetic analyses have great prospects for tracking thermal changes.

In this study, we proposed a new method, thermal rock magnetic cycling (TRMC), which conducted critical rock magnetic properties at elevated temperatures during multiple heating-cooling cycles to provide deeper insight into the thermal alteration of bulk samples and individual magnetic components with different Curie temperatures in measured samples. We conducted the TRMC method on a Galapagos lava sample GA 84.6 (Wang & Kent 2013; 2021). The variation in hysteresis properties revealed that the corrected Arai plot of GA 84.6c contained two linear segments with different palaeointensity values, but both were biased by thermophysical alteration. To further test the effectiveness of the above method, we utilized the TRMC method to evaluate the thermal stability of a historical lava sample (HS 2) from Mt Lassen during high-temperature heating experiments, which helped us to detect thermal changes and interpret the changes in the TRM unblocking spectrum of palaeointensity specimen. As a new method, the TRMC experiment can track thermal alteration details, which can help us assess the thermal stability of palaeointensity specimens, interpret palaeointensity estimates in previous studies and preselect palaeointensity samples in new palaeofield strength studies.

### 2 MATERIALS AND METHODS

### 2.1 Lava samples

Lava samples from the GA-X site on Floreana Island in the Galapagos Archipelago (Fig. S1) provide a valuable low-latitude record of the Santa Rosa Excursion event during the Matuyama chron. This event has been dated to 925.7  $\pm$  4.6 ka based on  $^{40}$ Ar/ $^{39}$ Ar age determinations (Balbas et al. 2016) and has an associated palaeointensity record of 4.23  $\pm$  1.29  $\mu$ T (Wang & Kent 2013; 2021). Although the pTRM check of the critical specimen GA 84.6c from the GA-X site passed, it failed to provide a reliable palaeointensity record. For this study, we chose sister specimens of GA 84.6 for electron probe micro-analyser (EPMA) analysis and comprehensive thermal rock magnetic cycling (TRMC) measurements. These specimens were cut from 10-mm-diameter half-cylinder specimens cut along the edge of palaeointensity specimen GA 84.6c (Wang & Kent 2013, 2021; Fig. S2). We also measured conventional rock magnetic curves at room temperature on these fresh specimens to verify the consistency of hysteresis behaviour in GA 84.6 sister specimens using the Day plot (Fig. S3).

To further test the effectiveness of our TRMC method for palaeointensity interpretations, we conducted the proposed experiment on another historical lava specimen, HS 2-8C. On 19 May 1915, a small eruption occurred at Mt Lassen in northern California. The geomagnetic field strength at the eruption site was 54 μT (Coe et al. 2004). Coe et al. (2004) collected samples from the 1915 Mt Lassen dacite flow to obtain the hysteresis behaviour from rock magnetic experiments and extract the expected palaeointensity record using the Thellier method. Their results indicated that the primary magnetic carriers within sample HS 2 were non-single-domain (non-SD) titanomagnetite grains and obtained a relatively accurate palaeointensity of 45  $\mu$ T (Coe et al. 2004). Additionally, Coe et al. (2004) also observed that the room-temperature remanences and coercivities slightly changed after repeated heating-cooling treatments, especially after heating from 400 to 600 °C. These findings prompted us to use the new TRMC method to evaluate the impact of thermal changes on palaeointensity estimates within the 1915 Mt Lassen sample.

### 2.2 Rock magnetic measurements and EPMA analysis

To identify the composition and size distribution of magnetic carriers within the Galapagos lava sample, we measured low-temperature thermal fluctuation tomography (LT-TFT, Jackson et al. 2006) curves on a fresh specimen GA 84.6v from 10 to 320 K for every 10 K using the Quantum Designs Magnetic Properties Measuring System (MPMS) in the Institute for Rock Magnetism (IRM), the University of Minnesota. Another specimen, GA 84.6u, was chosen for EPMA analysis and back-scattered electron (BSE) imaging using an electron probe microanalyser at Wuhan Sample Solution Analytical Technology Co., Ltd, Wuhan, China. The analysis was conducted using the JXA-8230 model from JEOL with a 1  $\mu$ m beam diameter and either 15 or 20 kV accelerating voltage. After two heating-cooling cycles with a target temperature of 607 °C, the same microscopic analysis was conducted on specimen GA 84.6w to detect potential thermal alteration. BSE imaging was also conducted on a fresh specimen and an after-heated specimen from sample HS 2, which may detect the thermal changes after high-temperature heating treatments.

In addition, we conducted low-field thermal magnetic susceptibility measurements ( $\kappa$ –T curves) in Argon on a powdered bulk sample of GA 84.6 using an AGICO KLY-3 Kappabridge equipped with a high-temperature furnace at the Palaeomagnetism and Geochronology Laboratory at the Institute of Geology and Geophysics, Chinese Academy of Sciences. In order to gain more insights into the thermal alteration characteristics, we conduct high-temperature rock magnetic measurements on additional fresh ~20 mg specimen GA 84.6w on a high-temperature measurements system in the Institute for Rock Magnetism (IRM), the University of Minnesota. We calculated the low-field susceptibility ( $\kappa_{LF}$ ) from the hysteresis loops measured at elevated temperatures from room temperature to 607 °C for every 20 °C. Then, we repeat the 25 °C to 607 °C measurements after the first heating treatment, which allows us to compare the  $\kappa_{LF}$  values of the initial state to the after-heated state.

### 2.3 Thermal rock magnetic cycling (TRMC) experiment

We performed the newly developed TRMC experiment on a Galapagos lava specimen GA 84.6v to track the thermal alteration in detail. We used a Lake Shore vibrating sample magnetometer (VSM 8604) at the China University of Geosciences (Wuhan, Fig. S4), equipped

with a Model 86-OVEN high-temperature oven to measure hysteresis loops, back-field direct current demagnetization (DCD) curves and first-order reversal curves (FORCs, Pike *et al.* 1999; Roberts *et al.* 2014) at elevated temperatures from 25 °C to each target temperature (100 °C, 200 °C, 300 °C, 400 °C, 450 °C, 500 °C, 550 °C, 575 °C) every 25 °C. To track the thermal alteration after the first heating to 575 °C, we repeat the specimen heating from room temperature to 575 °C (Fig. 1). The above TRMC procedure for specimen GA 84.6v included nine heating-cooling cycles and required over 300 hr of experimental time (Fig. 1).

During the TRMC experiment (Fig. 1), all rock magnetic curves were measured in a maximum applied field of 1.5 T. Critical parameters such as saturation magnetization  $(M_s)$ , saturation remanent magnetization  $(M_{rs})$  and magnetic coercivity  $(B_c)$  were extracted from corrected hysteresis loops using high-field linear slope correction. The DCD measurement procedure was modified to obtain high-resolution DCD curves, and remanent coercivity  $(B_{cr})$  was extracted from these curves. We also calculated the low-field susceptibility ( $\kappa_{LF}$ ) from the hysteresis loops after each heating-cooling cycle. The coercivity distribution of GA 84.6v was derived from DCD curves using the cumulative log Gaussian (CLG) model (Robertson & France 1994; Heslop et al. 2002) and skew-normal distribution model (MAX UnMix web application, Maxbauer et al. 2016) to analysis the magnetic constituents contained in the measured specimen. FORC measurements used a field increment of 2 mT and an averaging time of 1 s, and the software package FORCinel v3.06 (Harrison & Feinberg 2008) was used to calculate the FORC diagrams. We additionally used an Agilent molecular pump to reduce the inner furnace pressure from 101.325 kPa (atmospheric pressure) to about 10<sup>-7</sup> kPa during the TRMC experiment (Fig. S4c). At the same time, a flow of 99.99 percent high-purity inert argon gas was inserted at a rate of 80 to 130 cc/min into the sample space to avoid severe oxidation of the measured specimen (Fig. S4e).

Considering the relatively high thermal stability of the 1915 Mt Lassen sample, we perform a simplified TRMC procedure on specimen HS 2–8C. We modified the measured temperature intervals from 25 to 50 °C and selected a target temperature range from 100 to 600 °C at 100 °C intervals, which reduced the experimental time to less than 80 hr. We also used the VSM 8604 equipped with high-temperature measurement instruments (e.g. model-86 OVEN, Agilent molecular pump, as shown in Fig. S4) at the China University of Geosciences (Wuhan) to measure hysteresis loops, DCD curves, and FORCs from room temperature to each target temperature (100 °C, 200 °C, 300 °C, 400 °C, 500 °C, 600 °C and 600 °C). This entire set of TRMC experiments consists of seven heating-cooling cycles, and all rock magnetic curves were measured in a maximum applied field of 1.5 T.

### 3 RESULTS

### 3.1 Thermal alteration analysis for Galapagos lava sample GA 84.6

### 3.1.1 Magnetic carriers and thermophysical alteration

The results of EPMA analysis and BSE imaging of specimen GA 84.6u reveal micron-sized iron oxide particles (Figs 2a, b and S5) dominantly composed of titanomagnetite, with a maximum titanium content of almost 0.6 (Table S1). These particles commonly display extensive exsolution features, with ilmenite divided into regions with particle sizes of less than 10  $\mu$ m, or even 1  $\mu$ m, as a

### Thermal Rock Magnetic Cycling experiment for GA 84.6v

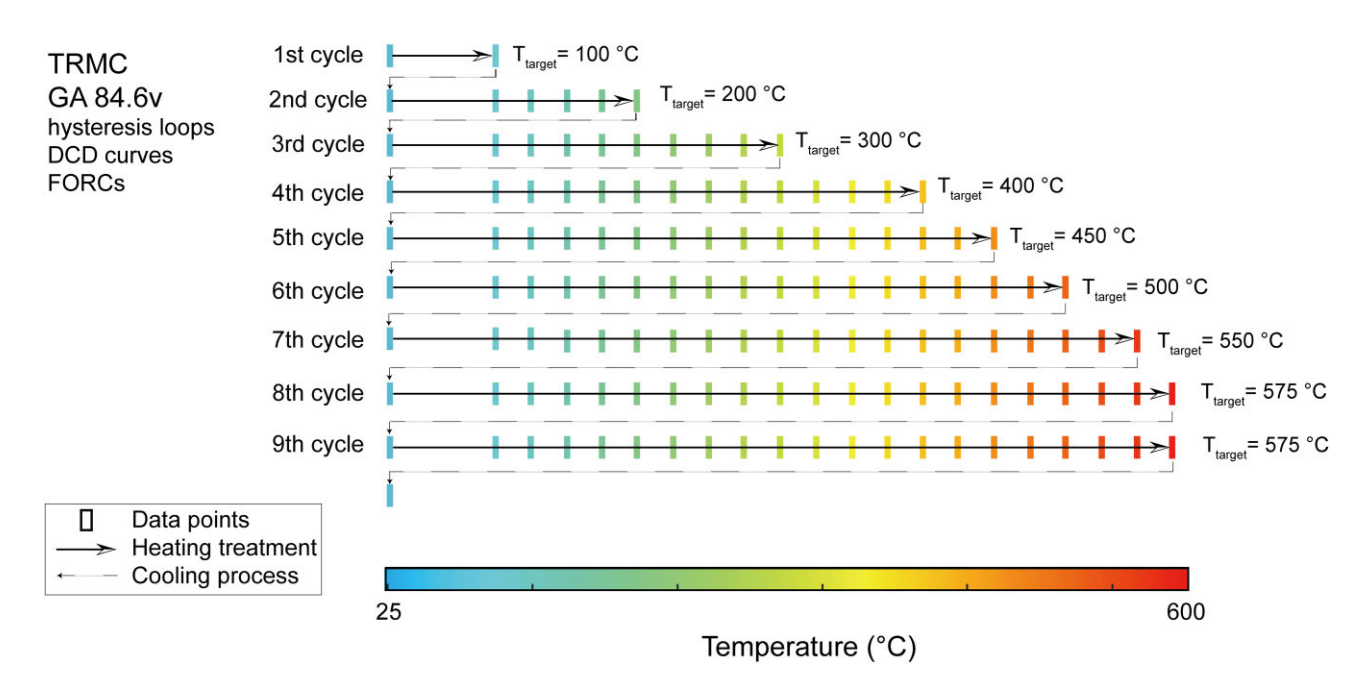


**Figure 1.** Schematic diagram of the thermal rock magnetic cycling (TRMC) experiment made at elevated temperatures for GA 84.6v. The TRMC experiment consisted of hysteresis loops, DCD curves and FORCs measurements. These were conducted at temperatures starting from room temperature up to target temperatures (100 °C, 200 °C, 300 °C, 400 °C, 450 °C, 500 °C, 550 °C, 575 °C and 575 °C) in increments of 25 °C. After each heating-cooling cycle, the sample was cooled to room temperature for the next heating-cooling cycle. Coloured squares represent the measured rock magnetic curves at corresponding heating temperatures. Numbers on the left label the heating-cooling cycles, while the target temperatures are labelled on the right. Black arrows represent heating treatments, and grey dashed arrows represent the cooling process when no measurements were made.

result of deuteric oxidation (Fig. 2b). This produced low-titanium magnetite particles (Table S1). The Curie temperature near 580 °C from the temperature dependence of magnetic susceptibility ( $\kappa$ –T) curves (Fig. 2e) and the Verwey transition near 120 K (Fig. S6) also indicates that the dominant magnetic carrier within GA 84.6 is magnetite or low-titanium magnetite in agreement with previous studies by Wang & Kent (2013, 2021).

After subjecting the specimen to two heating-cooling cycles with a target temperature of 607 °C, the composition and size distribution of iron-oxides in the heated specimen GA 84.6w is nearly the same as in the GA 84.6u in the BSE image (Figs 2c, d and S5). This consistency suggests that no significant thermochemical alteration occurred, such as oxidation induced by high-temperature treatments. This finding is consistent with the reversible heating-cooling curves of the thermomagnetic experiment for GA 84.6s (Wang & Kent 2013) shown in Fig. 2(g). The minimal changes in induced magnetizations suggest that the thermal alterations are predominantly thermophysical than thermochemical, as evidenced by the irreversible  $\kappa$ -T (Fig. 2e) and  $\kappa$ <sub>LF</sub>-T curves (Fig. 2f).

### 3.1.2 Tracking thermophysical alteration using the TRMC method

We extracted critical hysteresis parameters  $(M_{\rm s}, M_{\rm rs}, B_{\rm c} \text{ and } B_{\rm cr})$  from the rock magnetic curves obtained during the TRMC experiment (Fig. S7). The  $M_{\rm s}$  of GA 84.6v remained constant at each measured temperature across the different cycles, indicating again that no significant thermochemical alteration occurred in the measured specimen (Fig. 3a). The  $M_{\rm rs}, B_{\rm c}$  and  $B_{\rm cr}$  values measured after

heating to target temperatures of 100–400 °C (room temperature measurements in the second to fifth cycles) are all lower than the initial values (room temperature measurements in the first cycle, Figs 3b–d). After the target temperature reached 450 °C,  $M_{\rm rs}$  and  $B_{\rm c}$  measured at room temperature (6th cycle) increased by less than 3 per cent compared to the initial value. When the heating temperature reached 500 °C (7th cycle),  $M_{\rm rs}$ ,  $B_{\rm c}$  and  $B_{\rm cr}$  measured at room temperature strongly increased (Figs 3b–d) and reached a maximum after heating to 550 °C (8th cycle), significantly enhancing the remanence carrying capacity ( $M_{\rm rs}$ ) by 23.6 per cent (Fig. 3b). Although the values of  $M_{\rm rs}$  and  $B_{\rm c}$  began to decrease after the initial heating to 575 °C (9th cycle),  $M_{\rm rs}$  was still enhanced by 17.0 per cent compared to the initial state in room temperature measurements (Fig. 3b). After the second heating to 575 °C (9th cycle),  $M_{\rm rs}$  and  $B_{\rm c}$  increased to 13.1 and 38.7 per cent of the initial values, respectively.

The variations in the parameters described above indicate that thermophysical alteration of the measured specimen occurred throughout the heating treatment during the TRMC experiment. For target temperatures below 450 °C, the measured specimen undergoes thermophysical alteration involving domain structure changes, reducing the remanence carrying capacity. After GA 84.6v was heated to 450 °C, the  $M_{\rm rs}$  and  $B_{\rm c}$  began to increase. Severe thermal alteration occurs after heating to 550 °C due to changes in domain state (PSD to more SD behaviour), leading to a sharp enhancement of the remanence carrying capacity. Additionally, room-temperature  $\kappa_{\rm LF}$  values exhibit a reduced trend after 400 °C heating treatments (Fig. S8), which may originate from domain state changes after high-temperature heating treatments.

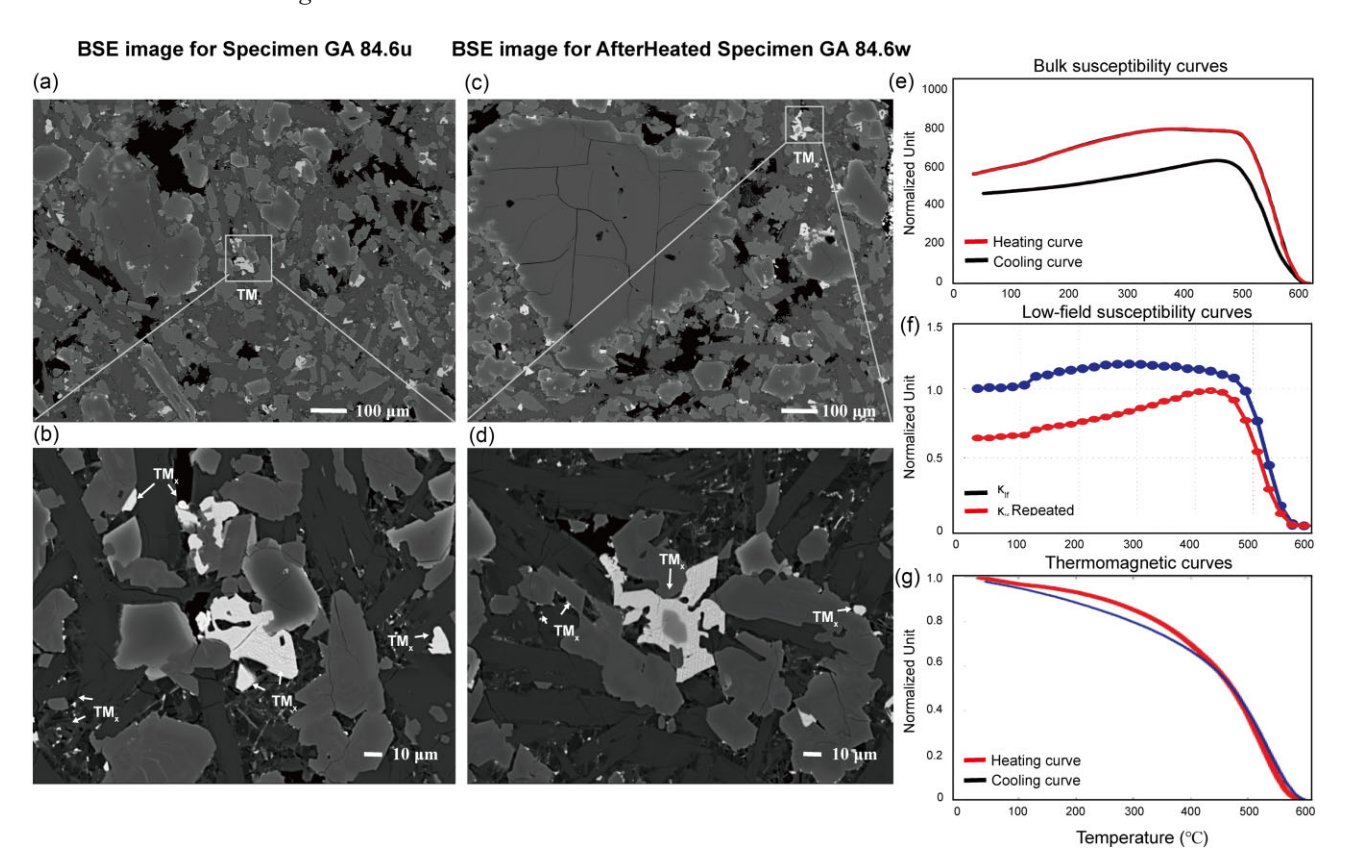


Figure 2. BSE images taken before ('u') and after ('w') heating specimens of GA 84.6 (a–d). The densely distributed micron-sized titanomagnetite (TM) grains typically exhibit extensive exsolution (a). Darker ilmenite divides primary titanomagnetite into brighter iron-rich regions due to deuteric oxidation (b). Microscale iron oxide grains are densely dispersed throughout the specimen (b). After high-temperature (607 °C) measurements, the magnetic mineral composition and particle size distribution in GA 84.6w closely resembled that of GA 84.6u (c, d). (e)  $\kappa$ -T curves (normalized to weight) for GA 84.6 subsamples. (f)  $\kappa$ LF-T curves (normalized to the initial  $\kappa$ LF value at room temperature) for GA 84.6w. (g) Thermomagnetic curves for GA 84.6s, with magnetization normalized to the initial MS of the fresh specimen. (g) Figure and caption are modified from fig. 3 of Wang & Kent (2013).

Furthermore,  $M_{\rm rs}$  dropped to  $10^{-7}$  Am² after the measured temperature first reached 550 °C in the seventh cycle (Fig. 3b), representing the value of saturation remanent magnetization carried by magnetic carriers with Curie temperatures above 550 °C in GA 84.6v. Moreover, we found that  $M_{\rm rs}$  and  $B_{\rm c}$  remained relatively constant as the specimen was heated to 550 °C for the first (7th cycle) to the third (9th cycle) time (Figs 3b and c), demonstrating that the magnetic carriers with high Curie temperatures (>550 °C) have high thermal stability. The variations in hysteresis behaviour of bulk specimen GA 84.6v at room temperature resulted from thermal alteration of the magnetic carriers with Curie temperatures below 550 °C.

We obtained two components (low-coercivity component, LC, and high-coercivity component, HC) unmixed from DCD curves using skew-normal distribution and CLG distribution models (Figs S9 and S10). Fig. 4 shows the critical hysteresis parameters ( $B_{\rm crL}$ ,  $B_{\rm crH}$ , SIRM<sub>L</sub>%, SIRM<sub>H</sub>% obtained from the skew-normal model;  $B_{\rm crL}$ ,  $B_{\rm crH}$ , SIRM<sub>L</sub>, SIRM<sub>H</sub> obtained from the CLG model) of each magnetic component contained in GA 84.6v. When the target temperature was below 500 °C, both values of SIRM<sub>L</sub> and SIRM<sub>H</sub> decreased (Fig. 4). Therefore, the reduced remanence of the measured specimen in this lower temperature range (<500 °C) originating from domain structure changes in the LC and HC. Considering the room temperature SIRM<sub>H</sub> increases sharply, and the value of SIRM<sub>H</sub>% is enhanced to 70 per cent when the target temperature exceeds 500 °C, we suggest that HC minerals mainly

dominate the hysteresis properties of the bulk specimen, especially after the high-temperature heating process higher than 500 °C (Fig. 4).

FORC measurements were conducted simultaneously during the TRMC experiment. For target temperatures below 450 °C, FORC diagrams from the first to the fifth cycles displayed a consistent vertical spread along the  $B_{\mu}$ -axis and a low-coercivity signal (Fig. 5), indicating that subtle thermophysical alterations during low-temperature heating were not discernible in the FORC diagrams. A slight increase in coercivity was observed after heating the specimen to 450 °C, resulting in more SSD-like behaviour in the FORC diagrams (Fig. 5). For target temperatures exceeding 450 °C, FORC diagrams, measured at room temperature, revealed a closed-contour peak with extensive vertical and horizontal spreads (Fig. 5). This suggests strong thermal changes, leading to a shift in the domain state towards a more SD-like behaviour, as evidenced by the rapid movement of hysteresis parameter ratios from the PSD to more SD-like behaviour in the Day diagram (Fig. 5).

Consequently, thermophysical alteration is primarily driven by changes in the domain structure of the bulk specimen when target temperatures remain below 450 °C, resulting in a reduced remanence carrying capacity. Upon reaching a target temperature of 450 °C, the remanence carrying capacities of GA 84.6v start to increase sharply, largely attributed to the thermal alteration of the HC. Moreover, as the measured temperature approached 550 °C—near the Curie temperature of most meta-stable magnetic particles within

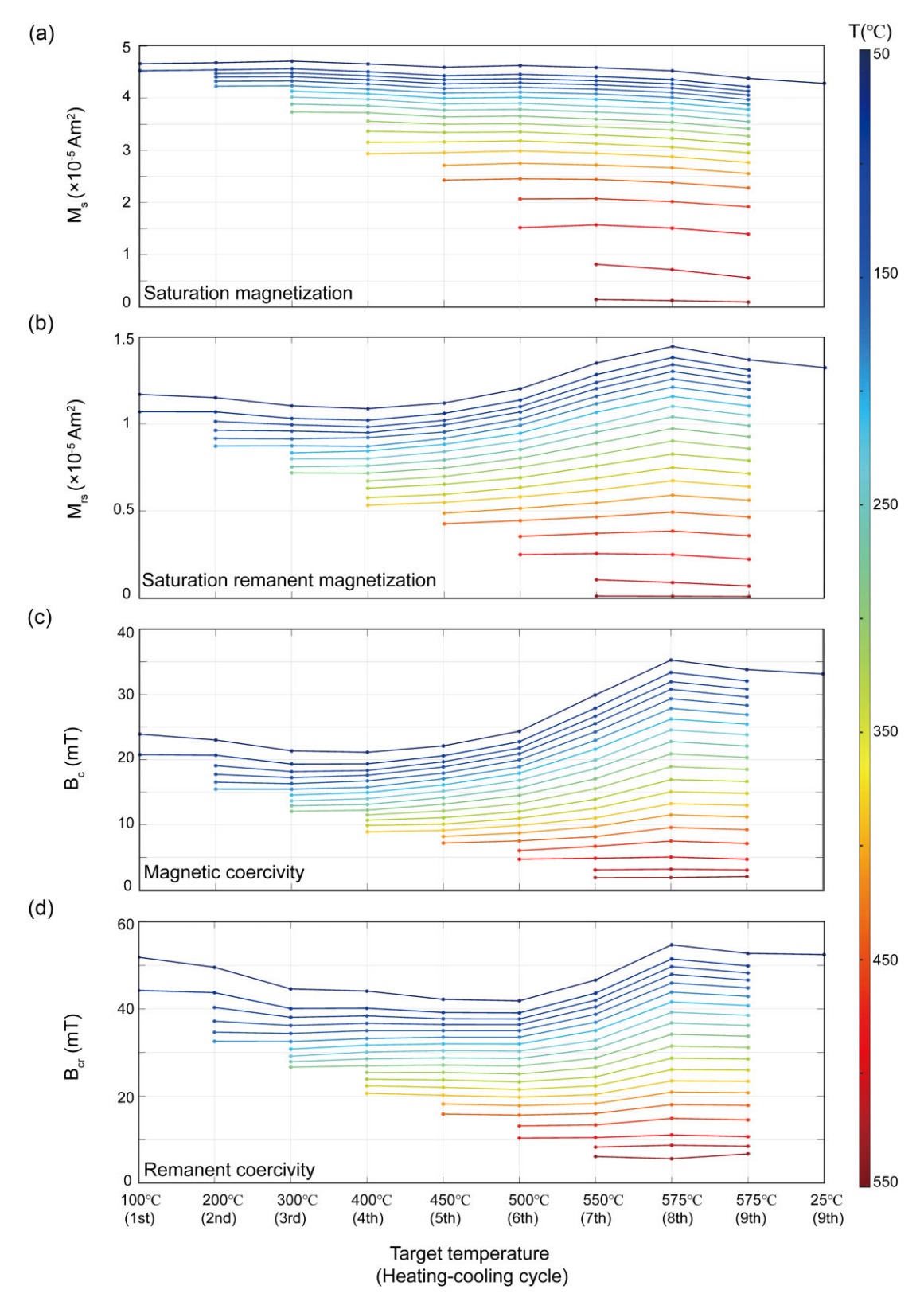


Figure 3. Hysteresis parameters  $(M_s, M_{rs}, B_c \text{ and } B_{cr})$  of specimen GA 84.6v at various temperatures from the TRMC experiment. The *Y*-axes represent the values of  $M_s$  (a),  $M_{rs}$  (b),  $B_c$  (c) and  $B_{cr}$  (d), respectively. The *X*-axes represent the target temperatures from 100 to 575 °C, including nine heating-cooling cycles. Measurements were conducted from room temperature up to 575 °C during the ninth cycle (the last cycle), after which the specimen was cooled back to room temperature for a final measurement, completing the TRMC experiment. Each data point on the series corresponds to hysteresis parameters measured from 25 °C to a target temperature. Points with the same fill colour were measured at the same temperature in different heating-cooling cycles.

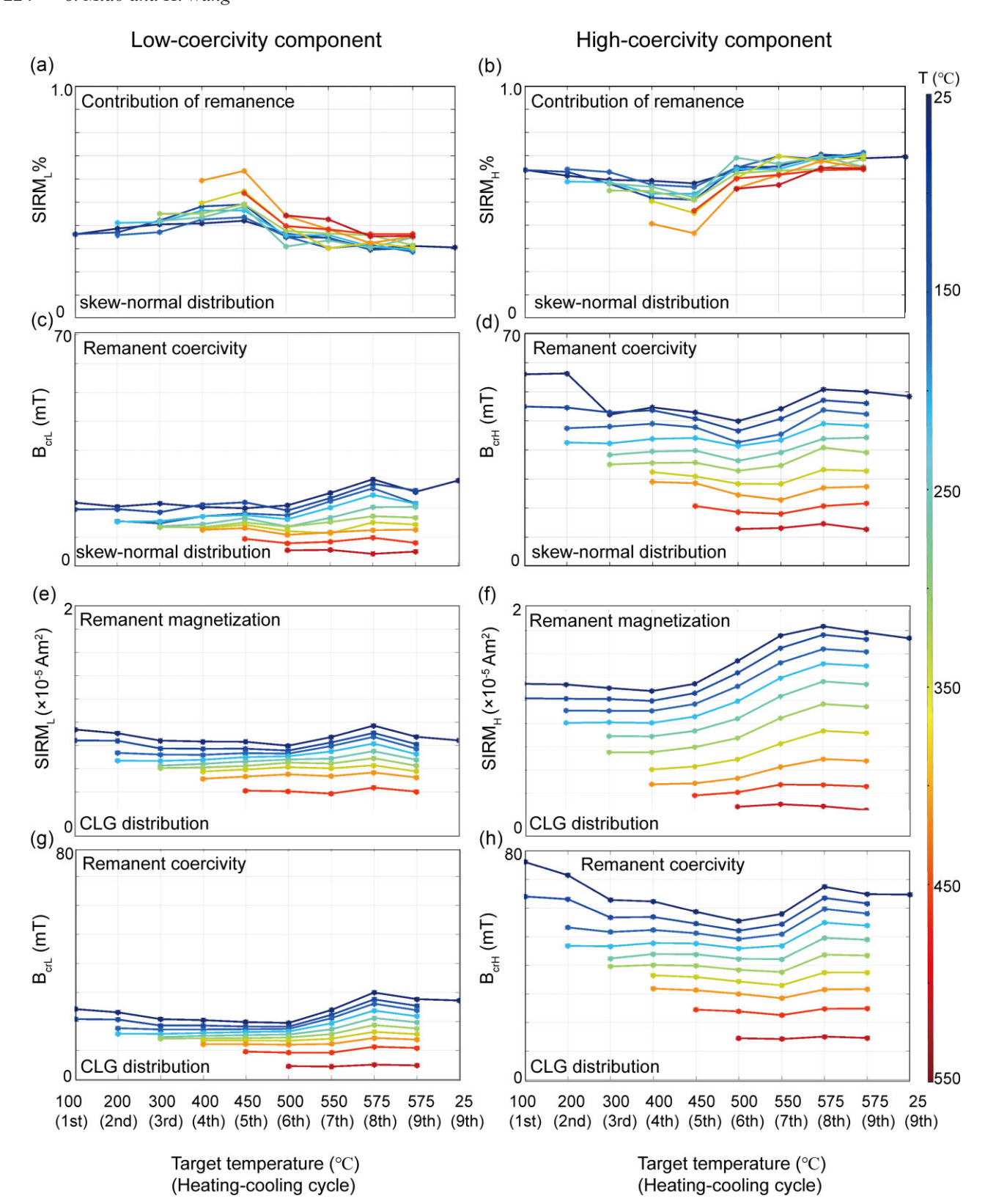
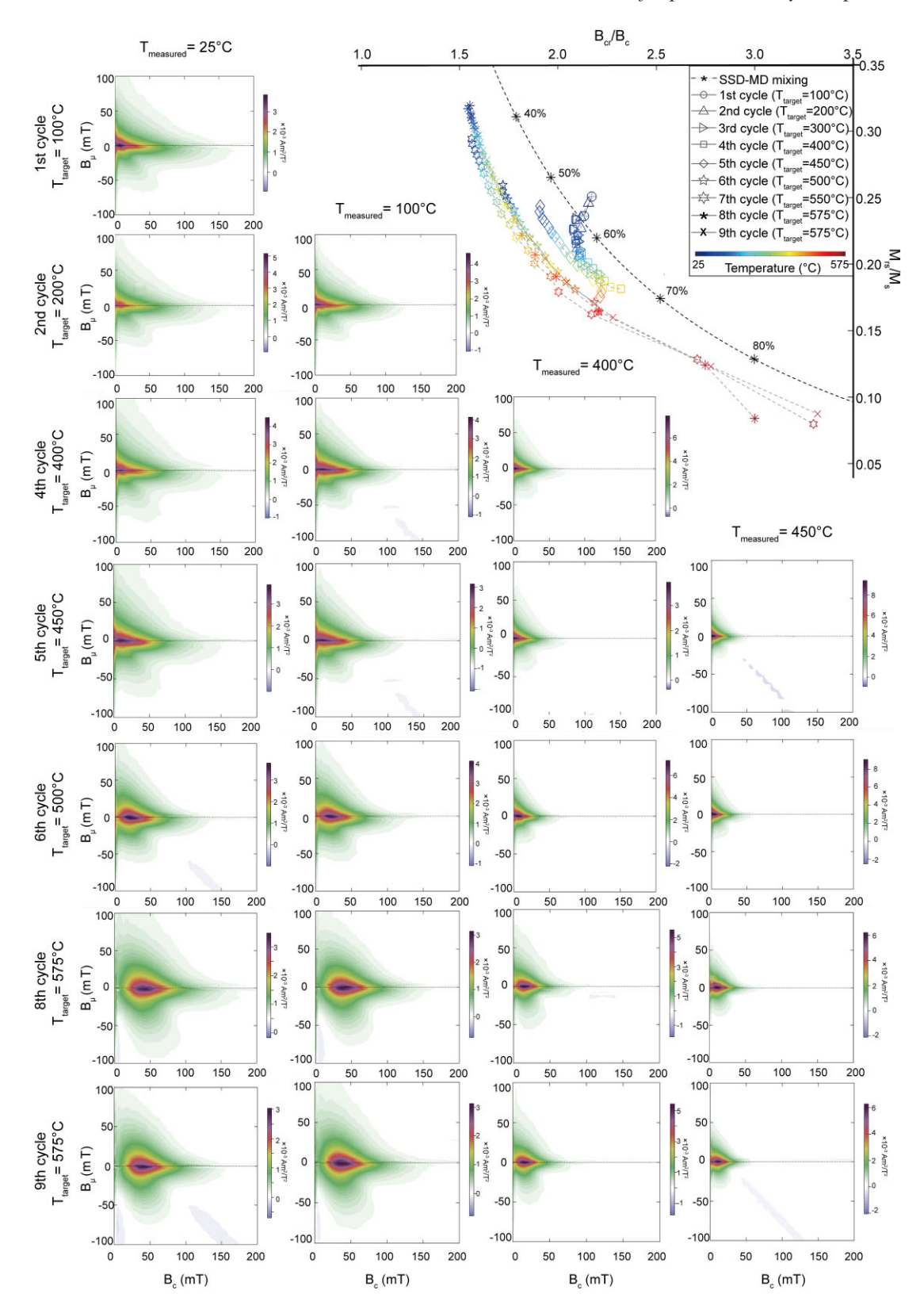


Figure 4. (a–d) Unmixing coercivity spectrum using the MAX UnMix web application (Maxbauer *et al.* 2016) based on the skew-normal distribution model. (a–d) Hysteresis parameters of the low-coercivity (a, c) and high-coercivity component (b, d) at elevated temperatures from the TRMC experiment for every 100 °C. The *X*-axes represent the target temperature. *Y*-axes represent the contribution of remanence (SIRM<sub>L</sub>% & SIRM<sub>H</sub>%) and remanent coercivity ( $B_{crL}$  and  $B_{crH}$ ) for the LC (a, c) and the HC (b, d). (e–h) Decomposing coercivity spectrum using the CLG model and extracting critical hysteresis parameters ( $B_{crL}$ ,  $B_{crH}$ , SIRM<sub>L</sub> and SIRM<sub>H</sub>) of the LC (e, g) and HC (f, h). The variations in remanent coercivity of two components from different models during the TRMC experiment are comparable, such as room-temperature  $B_{crH}$  obtained from skew-normal and CLG models are all reduced when the heating temperatures are lower than 500 °C (d and h), which indicates that the reliability of the two models for analysing magnetic constituents within GA 84.6v.



**Figure 5.** FORC diagrams for specimen GA 84.6v at elevated temperatures during the TRMC experiment. FORC diagrams measured at the same temperature are displayed in the same column, ranging from room temperature to 450 °C. Each row of FORC diagrams represents FORCs measured across a heating-cooling cycle at target temperatures from 100 to 575 °C. The software package FORCinel v3.06 (Harrison & Feinberg 2008) was used to calculate the FORCs (field increment of 2 mT, 201 FORCs) with a smoothing factor of 4. The inset diagram in the top right-hand corner represents the Day plot of GA 84.6v at elevated temperatures from the TRMC experiment. The different symbols represent the hysteresis parameters measured from different heating-cooling cycles, and percentages on the dashed curve represent modelled volumes of the MD contribution to SSD-MD mixing curve #3 (Dunlop 2002). The FORC diagrams measured at other heating temperatures are shown in Fig. S11.

GA 84.6v—the hysteresis parameters stabilized, indicating the thermal stability of magnetic carriers with higher Curie temperatures.

### 3.2 Thermal alteration analysis for 1915 Mt Lassen sample HS 2 $\,$

In the historical lava specimens of HS 2, primary titanomagnetite exhibits constant near-homogeneous features in the fresh specimen (Fig. 6a) and the after-heated specimen (Fig. 6b). For another lava specimen, HS 2–8C, we extracted critical hysteresis parameters ( $M_s$ ,  $M_{rs}$ ,  $B_c$  and  $B_{cr}$ ) from rock magnetic curves (Fig. S12) during the TRMC experiment to detect thermal changes within the measured specimen. Considering changes in the saturation magnetization are considered to best detect thermochemical alteration, the temperature dependence of  $M_s$  is shown in Fig. 7(a). Additionally, the TRMC results of the Galapagos lava sample indicated that  $M_{rs}$  values are valuable markers of variations in the remanence carrying capacity and domain state of the measured samples, which should be regarded as the most important parameter to analyse. Thus, we prioritized establishing the temperature dependence of  $M_{rs}$  in Fig. 7(b). Other hysteresis properties ( $B_c$  and  $B_{cr}$ ) are shown in Fig. S13.

Fig. 7(a) shows that the  $M_s$  of HS 2–8C remains constant at a given temperature over different heating-cooling cycles, indicating that no significant thermochemical alteration occurred. The  $M_{rs}$ measured after heating to target temperatures of 100-300 °C (room temperature measurements made at the second to fourth cycles) are relatively close to the initial value (Fig. 7b). When the target temperature reaches 400 °C, the room-temperature  $M_{\rm rs}$  (5th cycle) begins to increase and reaches a maximum value after the first heating to 600 °C (7th cycle, Fig. 7b). We determined that specimen HS 2-8C has remarkable thermal stability for target temperatures below 400 °C. Slight thermal-physical changes occurred in the specimen after heating to target temperatures reaching 400 °C. The value of  $M_{\rm rs}$  subsequently increased as a result of domain structure changes, weakly enhancing the remanence carrying capacity of HS 2-8C. The above thermal change details also lead to relatively constant values of hysteresis ratios  $(M_{rs}/M_s, B_{cr}/B_c, Fig. 7c)$  and room temperature  $\kappa_{LF}$  curve (Fig. S8).

Additionally, we can determine the thermal stability of each magnetic component with a distinct Curie temperature in HS 2–8C by monitoring the difference in properties obtained at two adjacent measured temperatures in each cycle, which is defined as  $M_{\rm rs,ycle}^{\rm measured \, temperature}$  (Fig. 7b). For instance, The values  $M_{\rm rs,lst}^{25-100}$ ,  $M_{\rm rs,2nd}^{100-200}$ ,  $M_{\rm rs,3rd}^{200-300}$  and  $M_{\rm rs,4th}^{300-350}$  remained relatively constant from the first to the seventh cycle, indicating stable remanence carrying capacities of magnetic minerals with lower Curie temperatures (25–350 °C). The slightly increased  $M_{\rm rs}^{350-500}$  values revealed that the variation in room temperature remanence resulted from the thermal alteration of magnetic minerals with Curie temperatures between 350 and 500 °C (Fig. 7b).

Fig. 7(d) shows that the fresh specimen has a typical MD FORC diagram dominated by a low-coercivity signal with a vertical spread along the  $B_{\mu}$ -axis, with similar distributions in the FORC diagrams measured after different cycles (Figs 7e–h). This consistency indicates that the weak thermophysical alteration after high temperatures cannot be detected by FORC diagrams. We also showed all the FORC diagrams in Figs S14 and S15.

In summary, for specimen HS 2–8C, slight thermophysical alteration occurred when target temperatures reached 400 °C, resulting in an increased remanence carrying capacity. We also isolated the

thermal stable magnetic component with the Curie temperatures between 25 and 350 °C. Based on the above thermal alteration analysis for specimens GA 84.6v and HS 2–8C, the TRMC is a powerful method that can track the cause and the process of thermal alteration of bulk specimens and utilizes critical hysteresis properties measured at elevated temperatures to assess the thermal stability of individual magnetic components with different Curie temperatures within each specimen. These findings are expected to evaluate the thermal stability of palaeointensity specimens and help palaeointensity interpretations, which are less detailed in previous studies.

### 4 DISCUSSION

### 4.1 Using the TRMC method to track thermal changes for palaeointensity interpretations

### 4.1.1 Galapagos lava sample GA 84.6

To better understand the total thermal changes that occur during palaeointensity determinations, we examined the palaeointensity results for GA 84.6c (Wang & Kent 2013; 2021). We found that the original Arai diagram displays two-slope behaviour (Fig. 8a). Based on our TRMC results for GA 84.6v, the value of  $M_{\rm s}$  remains constant at a given measured temperature across the different cycles (Fig. 3a), indicating that no significant thermochemical changes occurred. The decreases in room temperature remanence and coercivity of GA 84.6v after each target temperature from 100 to 400 °C indicate that changes in the domain configuration are responsible for reducing its remanence carrying capacity (Figs 3b–d). Additionally, the Zijderveld diagram of the specimen GA 84.6b in Fig. 8(a) indicates no significant secondary components in the NRM in the 100–575 °C interval.

While the hysteresis parameters begin to increase when the target temperature hits 450 °C, the values of  $M_{\rm rs}$  and  $B_{\rm c}$  measured at room temperature remain relatively consistent with the initial state. No significant change in domain state occurs until the target temperature reaches 500 °C (Figs 3b and c). Based on the original Arai diagram of GA 84.6c, the remanence carrying capacity of the measured specimen appears relatively stable, with a slight reduction after heating to temperatures below 500 °C. This leads to a decline in the pTRM-gaining ability of GA 84.6c in this lower temperature range, causing the NRM unblocked to exceed the pTRM imparted by the experimental field. This results in an overestimated palaeointensity value of 28.33  $\mu$ T (Fig. 8a).

When the target temperature reaches 500 °C, a pronounced increase in  $M_{\rm rs}$  at room temperature measurements indicates changes in domain states (moving from PSD to more SD-like behaviour). This leads to a sharp increase in remanence carrying capacity (Figs 3b and 5). In the original Thellier-Coe palaeointensity measurements, this thermophysical alteration shallower the NRM-pTRM slope and underestimated palaeointensity fitting by the high-temperature range ( $\geq$ 500 °C, Fig. 8a).

After the original Thellier-Coe experiment, Wang & Kent (2021) developed the RESET method, which involves subjecting a measured specimen (GA 84.6c) to a total TRM (tTRM) from the Curie temperature in a known laboratory field. The same palaeointensity procedure is then repeated (Fig. 8b), and a corrected Arai diagram is created by plotting the NRM remaining against the tTRM unblocking (Fig. 8c). The thermal changes of the measured specimen after the original Thellier-Coe experiment will lead to variations in the obtained tTRM unblocking spectrum, which may lead to

### (a) BSE image for unheated specimen

### (b) BSE image for heated specimen

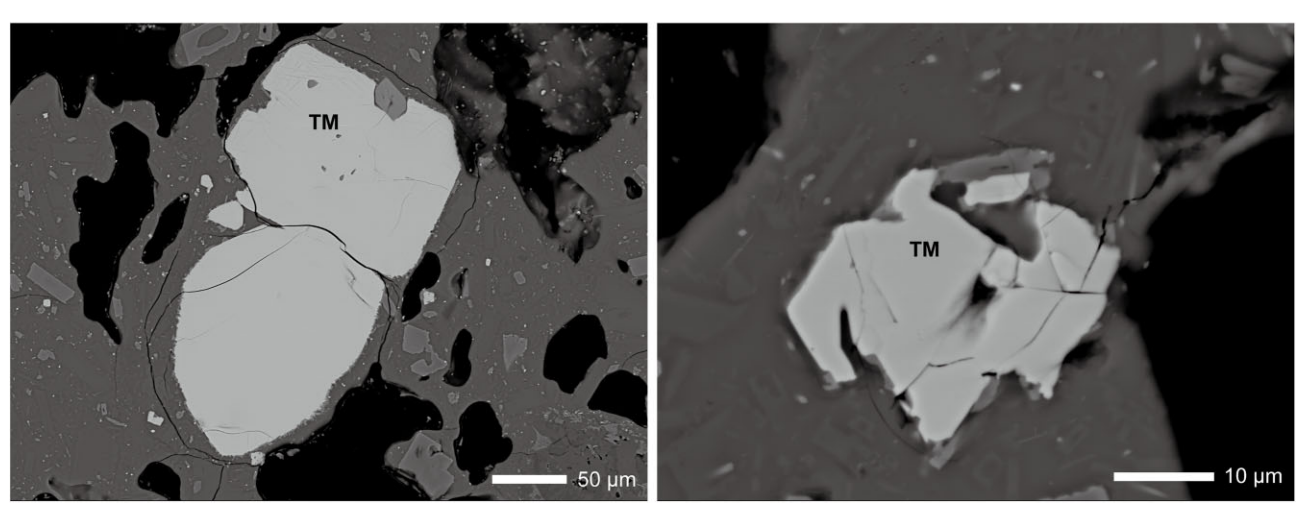


Figure 6. BSE images were taken before ('HS 2a') and after ('HS 2b') heating specimens of HS 2. The micron-sized titanomagnetite (TM) grains typically exhibit near-homogeneous features (a). There were no notable changes in the composition and size distribution of magnetic minerals after heating near the Curie temperature in HS 2b (b).

non-linear corrected Arai plots and biased palaeointensities. The TRMC results showed that the  $M_{\rm rs}$  of GA 84.6v increased by 13.1 per cent after the second heating to 575 °C (Fig. 3b), which indicates that the carrying capacities for remanent magnetization of the bulk specimen were enhanced. For LC and HC, the remanence carrying abilities are decreased and increased, respectively, derived from the significantly increased SIRMH along with a decrease in SIRM<sub>L</sub> after the second 575 °C heating treatments (Figs 4e and f). Therefore, the enhanced  $M_{rs}$  of the bulk specimen originated from HC with a thermal altered state, which reduced the effective grain size of magnetic carriers (PSD to more SSD behaviour) to promote remanence carrying capacities. Furthermore, a more than 30 per cent decrease in susceptibility of GA 84.6c after the original palaeointensity experiment (Wang & Kent 2013) also may demonstrate domain state changes for enhancement of remanence carrying capacities.

In the RESET-corrected Arai diagram (Fig. 8c), The LC minerals with lower Curie temperatures (<500 °C) displayed a reduction of remanence carrying capacities, leading to the acquisition of pTRM decrease during the tTRM obtained process after the original Thellier-Coe experiment (Fig. 8c). This process promotes NRM remaining to exceed the tTRM unblocking in this temperature intervals (0-500 °C) and biased palaeointensity to a higher value of  $26.57 \mu T$  (Fig. 8c). The thermal changes sharply enhanced the ability of HC to record remanent magnetization, such as the pTRM, which caused a shallower NRM-tTRM slope in this higher temperature range (500-575 °C, Fig. 8c). Consequently, the corrected Arai plot of GA 84.6c yielded two linear segments with distinct palaeointensity values (Fig. 8c), but both were biased by thermophysical alteration. The above findings are consistent with the TRM blocking spectrum of GA 84.6 shown in Wang & Kent (2013), which is mainly manifested as a minor decreased pTRM efficiency in 300-500 °C intervals and a sudden increase in pTRM recording capability in higher temperature segment (500-550 °C).

We isolated a stable magnetic component with a Curie temperature above 550 °C using the TRMC experiment (Fig. 3b), which may preserve a primary TRM. We estimated palaeointensity by fitting the corresponding segments (550–575 °C) on the corrected Arai plot and obtained a result of 4.50  $\mu$ T (Fig. 8c). Although the

palaeointensity value is consistent with the mean value for site GA-X (4.23  $\pm$  1.29  $\mu$ T, Wang & Kent 2013), the value may still be biased because it was obtained by fitting only two data points to calculate the palaeointensity.

### 4.1.2 1915 Mt Lassen sample HS 2

We track the entire sequence of thermal changes in a historical lava specimen (HS 2–8C) from Mt Lassen using the TRMC method to interpret the TRM unblocking spectrum of specimen HS 2–2C during palaeointensity experiments. Coe *et al.* (2004) collected samples from the 1915 Mt Lassen dacite flow to extract the expected palaeointensity record using the Thellier method. Their results indicated that nonlinear NRM-TRM curves, such as concave and S-shaped, are typical in Arai plots of the 1915 Mt Lassen samples (Coe *et al.* 2004). Although there is a large deviation in the palaeointensity values derived from low-temperature or high-temperature intervals, the slope calculated by connecting the initial and final data points from the Arai plots provided a more accurate average palaeointensity value of 52  $\mu$ T (Coe *et al.* 2004). For the specimen HS 2–2C, the slope of the line connecting the endpoints provided a relatively accurate palaeointensity value of 45  $\mu$ T (Coe *et al.* 2004).

Based on our TRMC results for HS 2-8C, a slightly underestimated palaeointensity record of HS 2-2C may have originated from the thermal instability of the measured sample. The increase in the remanence carrying capacity of the measured specimen after heating temperatures reached 400 °C during the TRMC experiment (5th cycle, Fig. 7b) led to the NRM being unblocked lower than the pTRM gained, resulting in a shallower NRM-pTRM slope and relatively biased palaeointensity record of 45  $\mu$ T (Coe et al. 2004). Our TRMC results indicate that the measured specimen remains thermally stable when the target temperature is below 400 °C. The demagnetization steps in the Thellier-type experiment show no significant secondary components in the NRM (Fig. 8d). Therefore, we may derive a more accurate palaeointensity value of 51  $\mu$ T by fitting the lower-temperature segment (≤360 °C) from the Arai plot (Fig. 8d), which is closer to the expected field strength (54  $\mu$ T). When the target temperature exceeds 400 °C, the increase in  $M_{\rm rs}$ 

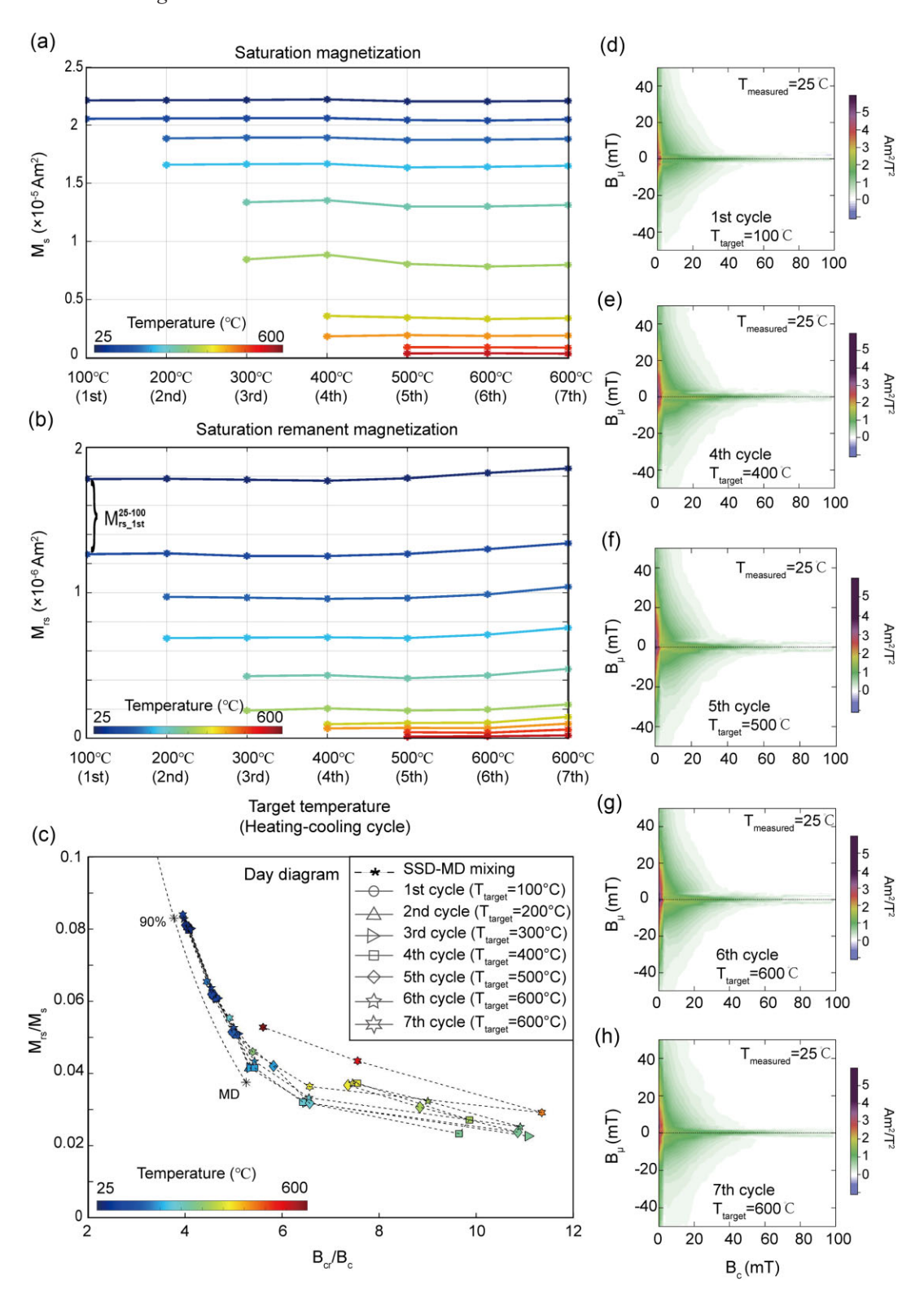
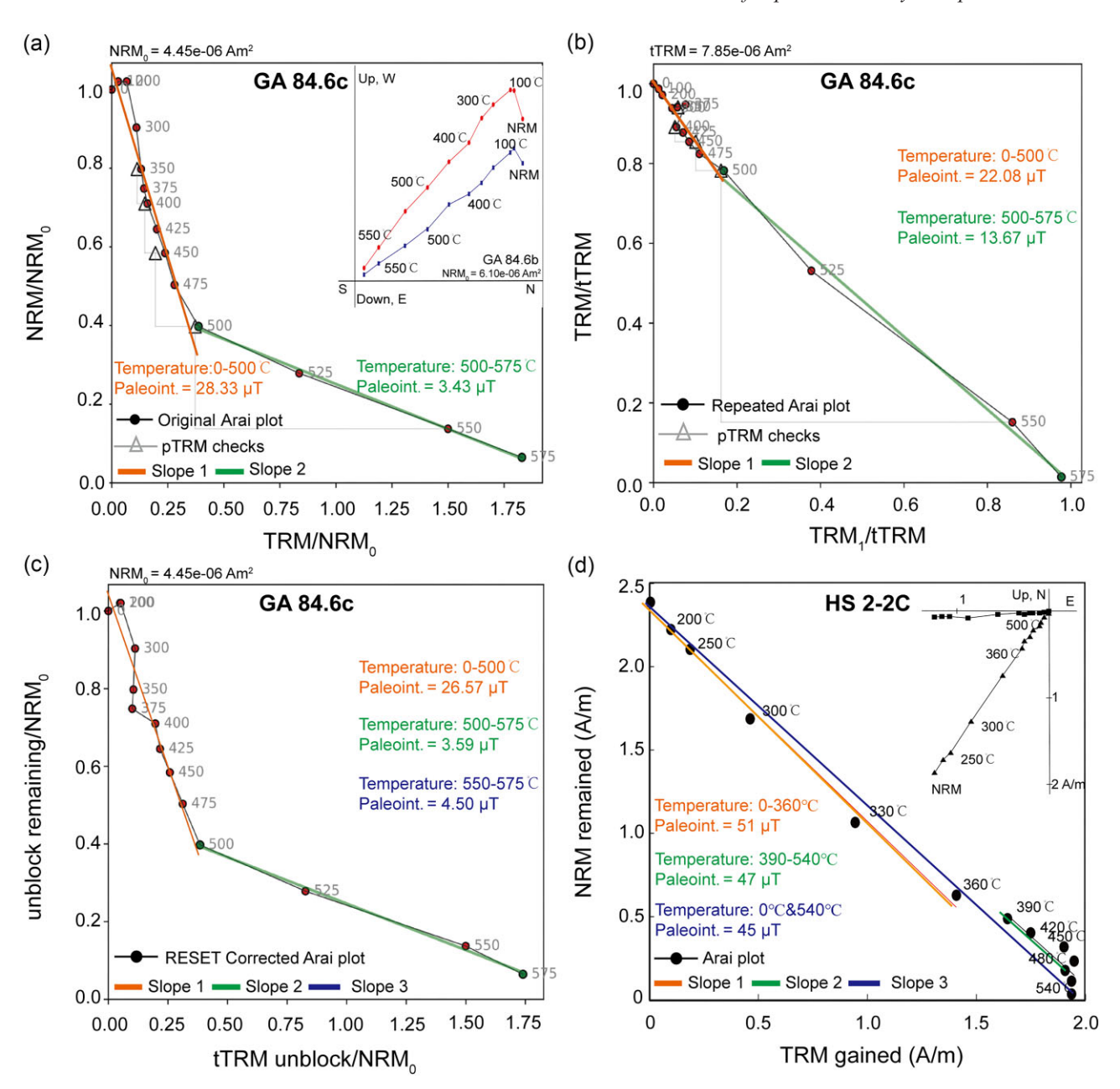


Figure 7. (a, b) Critical hysteresis parameters  $(M_s, M_{rs})$  for specimen HS 2–8C at elevated temperatures from the TRMC experiment. The Y-axes represent the values of  $M_s$  (a) and  $M_{rs}$  (b). The X-axes represent target temperatures ranging from 100 to 600 °C, including seven heating-cooling cycles. The measurements were conducted from room temperature to 600 °C in the seventh cycle (last cycle), then the specimen was cooled back to room temperature to complete the TRMC experiment, during which no measurements were made. The difference in  $M_{rs}$  obtained at two adjacent measured temperatures in each cycle is defined as  $M_{rs.cycle}^{2S-100}$ , such as the difference in  $M_{rs}$  obtained at two adjacent measured temperatures (25 and 100 °C) in the first cycle is defined as  $M_{rs.struct}^{2S-100}$  (b), which represents a decline of  $M_{rs}$  value from 25 °C measurements heating to 100 °C measurements. (c) Day plot of HS 2–8C at elevated temperatures from the TRMC experiment. The different symbols represent the hysteresis parameters measured from different heating-cooling cycles, and percentages on the dashed curve represent modelled volumes of the MD contribution to SSD-MD mixing curve #3 (Dunlop 2002). (d–h) FORC diagrams measured at room temperature from different heating-cooling cycles (first cycle and fourth to seventh cycles, respectively).



**Figure 8.** (a and b) Arai plots for GA 84.6c, with figures and captions modified from fig. 10 of Wang & Kent (2013). In both the original (a) and repeated (b) Arai diagrams, the orange line indicates palaeointensity estimates obtained by fitting the lower-temperature segment (<500 °C), and the green line indicates palaeointensity obtained by fitting the higher-temperature range (500–575 °C). Grey triangles represent pTRM checks. The inset diagram in the upper right-hand corner of (a) shows NRM thermal demagnetization vector diagrams for GA 84.6b. [figures and captions are modified from fig. 11 of Wang & Kent (2013).] Blue-filled data points indicate vector end-points projected onto the horizontal plane, red-filled data points indicate vector end-points projected onto the vertical plane, and numbers adjacent to data points are demagnetization temperatures. The X-axis of (b) is defined as TRM<sub>1</sub>/tTRM, which represents the TRM blocking spectrum of GA 84.6c during the repeated Thellier-Coe experiment. (c) The RESET-corrected Arai diagram of GA 84.6c. The orange line represents a linear regression from 25 to 500 °C, and the green line represents a linear regression from 500 to 575 °C. The blue line represents a linear regression from 550 to 575 °C, which may correspond to the thermally stable component with a high Curie temperature (550–575 °C) in GA 84.6c. (d) Arai plot for HS 2–2C, with figures and captions modified from fig. 6b of Coe *et al.* (2004). The orange line indicates palaeointensity estimates obtained by fitting the low-temperature segment (<390 °C), and the green line indicates palaeointensity obtained by fitting the high-temperature range (390–540 °C). The blue line represents the slope calculated by linking the initial and the final data points from Arai plots. The inset diagram in the upper right corner shows the NRM thermal demagnetization vector diagram for HS 2–2C from the Thellier-type experiment.

at room temperature due to domain configuration changes leads to a slight increase in the remanence carrying capacity. In Thelliertype palaeointensity measurements, this thermophysical alteration results in a shallower NRM-pTRM slope and yields an underestimated value of 47  $\mu T$  at the high-temperature interval ( $\geq$ 390 °C, Fig. 8d).

Utilizing the TRMC results to examine the Arai plot, we observed that the S-shaped NRM-TRM curve arises from weak thermalphysical changes within HS 2-2C at target heating temperatures above 400 °C. The TRMC experiment comprehensively captures the entire thermal alteration of the 1915 Mt Lassen specimen (HS 2-8C), aiding in interpreting the TRM unblocking spectrum behaviour for specimen HS 2-2C. As MD grains are the primary magnetic carrier within the measured specimen, the MD effect may also contribute to the non-linear Arai plot and biased current palaeointensity value. However, the thermal changes in the measured sample are still a critical factor that cannot be ignored when analysing the fidelity of the palaeointensity estimates. Therefore, as a powerful method, the TRMC experiment can effectively identify the entire process of thermal alteration in rock magnetic specimens, which can be used to help interpret changes in the TRM unblocking spectrum during palaeointensity experiments and to obtain more accurate palaeointensity estimates from specimens with partial thermal stability.

### 4.2 Assessing the effectiveness of the TRMC method

Our TRMC experiment conducted hundreds of rock magnetic curves, offering comprehensive details about thermal alteration during heating treatment. Rapid hysteresis loop and remanent curve measurements yield diagnostic rock magnetic parameters (e.g.  $M_s$ ,  $M_{\rm rs}$ ,  $B_{\rm c}$  and  $B_{\rm cr}$ ) measured at room temperature and can capture the thermal alteration of samples after heating to each target temperature (Figs 3, 4 and 7). These room temperature outcomes aid in evaluating the thermal stability of measured samples and can help us interpret TRM unblocking spectrum shifts (Fig. 8). Moreover, the TRMC experiment also collected hysteresis properties at elevated temperatures, revealing changes in the hysteresis behaviour of various magnetic carriers with different Curie temperatures (Figs 3, 4 and 7). Therefore, we can study thermal alteration in each magnetic component with different Curie temperatures in measured samples and identify thermally stable components, such as those with high Curie temperatures (>550 °C) present in GA 84.6v (Fig. 3). By providing a method for tracking thermal alteration independent of palaeointensity experiments, the TRMC method can explore subtle, unrecognizable thermal alteration processes in less detailed palaeointensity measurements, which can help palaeointensity interpretations (Fig. 8).

Although the pTRM check for Galapagos lava specimen GA 84.6c passed, this specimen failed to provide a satisfactory palaeointensity estimate from the RESET method. In our TRMC experiments, we traced the thermophysical change details within the measured specimen GA 84.6v. These findings were then used to help evaluate the thermal stability and interpret the TRM unblocking spectrum in the palaeointensity results for GA 84.6c. Consequently, the TRMC method proposed here can assess the thermal stability of the rock magnetic specimens during the entire heating treatment, which can help us interpret the TRM unblocking spectrum of the palaeointensity specimens during the Thellier-type method.

The CAL check from the RESET palaeointensity experiment offers a more robust approach for tracking thermal changes and detecting alteration by assessing the linearity of the corrected Arai plot (Wang & Kent 2021). However, during palaeointensity experiments, the CAL check was also blind to those samples with proportional thermal changes, leading to a more linear Arai diagram, such as in GA 84.6c. Our studies indicate that the corrected Arai plot for

GA 84.6c yielded two linear segments and distinct palaeointensity values (Fig. 8c). However, both values were biased, caused by thermophysical alteration detected by the TRMC experiment. Once thermal alteration occurs, the TRMC method will detect it.

Conventional rock magnetic measurements, conducted before and after heating steps, were also used to monitor thermal changes in GA 84.6 (Wang & Kent 2021) and HS 2 (Coe *et al.* 2004). These room-temperature rock magnetic measurements can be used to evaluate the thermal changes in bulk samples post-heating but do not address the processes of thermal alteration in magnetic constituents with different Curie temperatures in a sample. The TRMC experiment not only detects the thermal changes in a sample after each heating treatment via room temperature measurements but also identifies the thermal stability of each mineral component with varying Curie temperatures through high-temperature measurements (Figs 3, 4 and 7).

### 4.3 Applications and limitations of the TRMC method

A potential pitfall in palaeointensity research is over-reliance on the linearity of the Arai diagram, especially for non-SD samples. This will lead to the thermal changes of samples that escaped in the most conventional check methods, resulting in biases in palaeointensity estimates. For example, while the original Arai plot of GA 84.6c contained two linear segments yielding different palaeointensity values (Fig. 8a), both were affected by previously undetected thermal alteration revealed by our TRMC experiment. We argue that such thermal alteration can remain hidden in more linear Arai plots. The TRMC method can detect the thermal alteration in detail and helps us gain deeper insight into the thermal stability of measured samples. It also offers a chance to interpret the variations in the TRM unblocking spectrum during palaeointensity experiments and assess palaeointensity estimates derived from relatively linear or dual-slope Arai plots frequently encountered in past studies, such as those in the Hawaii glassy volcanic specimen hw 120a4 [fig. 4 of Cromwell et al. (2018), Fig. S16a], the Pliocene lava sample LT 21– 5-1 from Iceland [fig. 6 of Tanaka & Yamamoto (2016), Fig. S16b], and late-Quaternary El Golfo sample EH 22-13A [fig. 5 of Monster et al. (2018), Fig. S16c].

Historical lava samples have been extensively investigated in recent decades, such as those from Hawaii (Yamamoto *et al.* 2003; Cromwell *et al.* 2015; Grappone *et al.* 2019; Jeong *et al.* 2021), Mt Etna (Calvo *et al.* 2002; Biggin & Dekkers 2007; de Groot *et al.* 2013; de Groot *et al.* 2014) and the Canary Islands (Calvo-Rathert *et al.* 2016). Although much effort has been made to utilize Thellier-series methods (Herrero-Bervera & Valet 2009; Cromwell *et al.* 2015; Jeong *et al.* 2021) to recover the palaeointensity values, the published palaeointensity determinations of some historical lava samples still deviate from the expected field strength.

de Groot *et al.* (2014) utilized magnetic force microscopy (MFM) to observe variations in magnetic domain structure in lava samples from Mt Etna to investigate the reason for the failure of palaeointensity estimates, which can be underestimated by nearly 50 per cent (Calvo *et al.* 2002; Biggin & Dekkers 2007; de Groot *et al.* 2013). They found that the domain structure starts to alter after heating to 120 °C, and the primary domain configurations become almost entirely rearranged in their pTRM state after heating to 250 °C (de Groot *et al.* 2014). A comparable situation exists for palaeointensity studies of historic lava flows from Hawaii. Cromwell *et al.* (2015) summarized all published palaeointensity results for the

1960 Kilauea lava flow and found that intensity estimates can deviate substantially from the expected value. Jeong *et al.* (2021) further showed that thermal alteration undetected by pTRM checks was one of the leading causes of bias in palaeointensity estimates in the 1960 Hawaii flow. Based on previous studies and current understanding of thermal alteration in the Mt Lassen specimen HS 2–8C, one of the main reasons for failing to recover the expected field strength is thermal alteration in historical lava samples (de Groot *et al.* 2014; Grappone *et al.* 2019; Jeong *et al.* 2021). Our TRMC method can track the course of thermal changes in rock magnetic specimens, which allows researchers to preselect thermally stable samples for new palaeointensity studies and understand the behaviour of Arai plots from previous palaeointensity experiments.

Although the accuracy of palaeointensity values can be readily assessed for historical lava samples based on the expected palaeointensities, the accuracy of geomagnetic field strength estimates from ancient rock samples, such as from the Precambrian, can only be surmised from experimental results (Halls *et al.* 2004; Smirnov 2005; Smirnov & Evans 2015). Therefore, there is an urgent need to develop more methods to assess the thermal stability of previously measured samples. The TRMC experiment proposed here can track the thermal alteration process in detail to preselect thermally stable samples for palaeointensity studies, thereby increasing success rates and helping us evaluate the fidelity of previous palaeointensity data.

Building on the above discussions, the TRMC method, as a standalone rock magnetic experiment distinct from Thellier-series experiments, reveals comprehensive details of thermal alteration in sister specimens. Although this information can help us understand the TRM unblocking spectrum of palaeointensity specimens, the TRMC method also has inherent weaknesses. As a comprehensive rock magnetic experiment, the TRMC method directly tracks the thermal changes of sister specimens to suppose the thermal stability of palaeointensity specimens. However, rock magnetic sister specimens may not completely represent the properties of the palaeointensity specimen because a lava flow may not be homogeneous (de Groot et al. 2014). It is necessary to verify the homogeneity of hysteresis behaviour among rock magnetic specimens prior to the TRMC and palaeointensity experiment. For example, we conducted conventional rock magnetic measurements before the TRMC experiment to verify the consistency in sister specimens of GA 84.6 (Fig. S3).

Among the critical hysteresis parameters, emphasizing analysis of the  $M_{rs}$  is crucial due to its sensitivity to stability in the remanence carrying capacity of samples during the TRMC experiment (Figs 3b and 7b). However, there are very different recording mechanisms between  $M_{rs}$  (obtained by a saturation field) and TRM (obtained by a weaker magnetic field, Thellier 1977). The variation in  $M_{\rm rs}$ does not directly reflect the changes in TRM, which is one of the potential limitations of the TRMC method. Considering the above situation, in our TRMC experiment, we usually uncovered variations in specimens' capacity for remanent magnetization using  $M_{rs}$ changes. Then, we analyse the reasons for the changes in the  $M_{\rm rs}$ value based on variations in the other properties  $(M_s, B_c \text{ and } B_{cr})$ , such as the magnetic domain state transition. For example, the magnetic domain state of GA 84.6v is more SD behaviour after the heating temperature reaches 500 °C, enhancing its remanence carrying capacity. Based on the above discussions, we can deduce the variation of the sample's carrying capacity for TRM, such as GA 84.6v, which has more SD behaviour in the after-heated state, leading to their increased carrying capacity for TRM. These insights may shed light on the thermal stability of the measured samples and can help us interpret the variations in the TRM unblocking

spectrum of palaeointensity specimens. Additionally, the TRMC experiment could not serve as the only standard for evaluating the fidelity of the palaeointensity estimates currently. It is necessary to combine traditional methods based on the TRM unblocking spectrum of palaeointensity specimens (Valet 2003), such as the pTRM check, with the TRMC method, which will help us understand the behaviour of the Arai plots more comprehensively and obtain abundant accurate palaeointensities for interpreting the evolution of the Earth's core dynamo.

The much longer experimental duration of the TRMC method may have led to unpredictable laboratory-induced thermal changes within the sister specimens, limiting the applicability of the TRMC experiments in palaeointensity studies. Therefore, a simplified experimental TRMC procedure is needed. For specimen HS 2-8C, we utilized an optimized TRMC procedure to track thermal changes. We modified the measured temperature intervals from 25 to 50 °C and selected a target temperature range from 100 to 600 °C at 100 °C intervals. This entire set of TRMC experiments takes less than 80 hr. Moreover, based on the FORC diagrams of GA 84.6v and HS 2-8C obtained during the TRMC experiments (Figs 5 and 7), we determined that FORC diagrams could not comprehensively detect thermal alteration during elevated heating steps. Considering the time-consuming FORC measurements, we only measure FORCs at critical temperature points to verify thermal alteration resulting from domain state changes, reducing the duration of the TRMC experiment to about 24 hr. Additionally, our TRMC method has great tracking of thermal changes in only two lava samples with titanomagnetite particles as the magnetic carrier mineral in this study. To further verify the effectiveness of the TRMC method for palaeointensity interpretations, we will select more abundant samples for TRMC experiments in future studies.

### 5 CONCLUSIONS

In this study, we developed a new comprehensive rock magnetic experiment, termed TRMC, to assess the thermal stability of measured samples and interpret palaeointensity results. We measured the rock magnetic properties of a Galapagos lava sample (GA 84.6) at elevated temperatures in multiple heating-cooling cycles, revealing that thermophysical alteration occurred throughout the treatment and led to the two-slope behaviour in the Arai plots for GA 84.6c. We also tracked the thermal changes in a Mt Lassen sample HS 2 using the TRMC method to test the viability of the above method. Results show that the TRMC method can track thermal alteration details in HS 2–8C, which allows us to evaluate the thermal stability of palaeointensity specimen (HS 2–2C) and helps us interpret the variations in the TRM unblocking spectrum during Thellier-series experiments.

The TRMC method utilizes critical hysteresis properties at elevated temperatures on sister specimens to track thermal changes in bulk samples and individual magnetic components with different Curie temperatures in a sample, which enables accurate palaeointensity estimates from samples with partial thermal stability and can be used to help palaeointensity interpretations. The TRMC method can also be widely used to preselect thermally stable samples in new palaeointensity studies to increase success rates. By conducting TRMC experiments combined with other conventional check methods, the entirety cause and the process of thermal changes within measured samples during palaeointensity experiments are expected to be revealed further, which facilitates abundant accurate

palaeointensities to study the behaviour of the geomagnetic field and the evolution of the Earth's core dynamo.

### ACKNOWLEDGMENTS

We thank Pierre Rochette for providing the Galapagos lava samples via Dennis V. Kent and Robert S. Coe for the Mt Lassen sample. We also thank Dennis V. Kent and Robert S. Coe for discussing and initially reviewing this paper. We are grateful to Huafeng Qin for measuring  $\kappa$ –T curves. We are grateful to Chen Wen, Yang Wu, Xuelong Jiang, Bincheng Hong, Haijun Li, Jianhong Luo, Xiaowei Chen and Ting Cao for their assistance with the TRMC experiment. We are also grateful to the Institute for Rock Magnetism (IRM) at the University of Minnesota for supporting Huapei Wang with a visiting fellowship, which allowed many of these rock magnetic measurements to be made. This research was supported by the National Natural Science Foundation of China (41874079 and 42030205).

### AUTHOR CONTRIBUTIONS

Huapei Wang developed the concept for this work and designed the rock magnetic experiments. Junxiang Miao conducted rock magnetic measurements and data analysis. Junxiang Miao and Huapei Wang wrote the paper.

#### SUPPORTING INFORMATION

Supplementary data are available at *GJIRAS* online.

**Figure S1**. Location map of the GA-X site from Floreana Island in the Galapagos Archipelago. (a) Map of Galapagos Archipelago. Figures and captions are modified from fig. 2 by Wang *et al.* (2015). (b) Sites GA-X is on Floreana Island. Our GA 84.6 sampling from site GA 84 is indicated by a red circle. Figures and captions are modified from fig. 1 of Wang & Kent (2013). White dots and black triangles are sampling sites from previous studies of Rochette *et al.* (1997) and Kent *et al.* (2010) that are not discussed in this paper.

Figure S2. 3-D sketch of the sample cutting strategy and divided sister specimens of GA 84.6. The specimens ("i", "s", "t", "u", "v", "w") are cut from a 10 mm diameter half-cylinder specimen for rock magnetic measurements, cut along the edge of palaeointensity specimen GA 84.6c (25-mm diameter cylinder, ~10–15 mm height). Another 10-mm diameter cylinder, GA 84.6X, is stored for future palaeomagnetic studies. The rest of the 25-mm diameter cylinder specimen GA 84.6c has been used for previous palaeointensity studies (Wang & Kent 2013, 2021). The sample-cutting strategy ensures that the rock magnetic specimens closely resemble the properties of the palaeointensity specimen. Figures and captions are modified from Wang & Kent (2013).

**Figure S3.** Homogeneity test for sample GA 84.6. We conducted hysteresis loop and remanence curve measurements on sister specimens ("i", "v", "w", "y") of the measured sample and plotted the hysteresis ratios on the Day diagram (a, b). The various GA 84.6 specimens have similar hysteresis behaviour in their initial state. (b) shows a smaller plot area. The percentages on the dashed curve in the Day diagrams are modelled volumes of the MD contribution to SSD-MD mixing curve #3 (Dunlop 2002).

**Figure S4.** Lake Shore vibrating sample magnetometer (VSM 8604) equipped with high-temperature measurement instruments for the TRMC experiments. (a) Lake Shore VSM 8604. (b, d) Model 86-OVEN high-temperature oven. (c) Agilent molecular pump. (e)

99.99 per cent high-purity inert gas Argon maintains at 80–130 cc min<sup>-1</sup> stream insert to the furnace.

**Figure S5.** Back-scattered electron (BSE) images of specimen GA 84.6u (a, c) and the after-heated specimen GA 84.6w (b, d). Micron-sized iron oxide particles with extensive exsolution from deuteric oxidation are abundant in the measured specimens. Magnetic mineral compositions and the particle size distribution in GA 84.6 are similar before and after heating treatment.

**Figure S6.** Low-temperature thermal fluctuation tomography (LT-TFT) measurements on a fresh Galapagos lava specimen GA 84.6v from 10 K ( $\sim$ -263 °C) to 320 K (near room temperature) for every 10 K. (a) Linear high-field slope corrected hysteresis loops, (b) DCD curves, (c)  $M_{\rm s}$ ,  $M_{\rm rs}$ ,  $B_{\rm c}$  and  $B_{\rm cr}$  versus temperature curves during heating treatment. (d) Hysteresis parameter ratios in the Day plot. Percentages on the dashed curve in (d) are modeled volumes of MD contribution to SSD-MD mixing curve #3 (Dunlop 2002), and the inset shows the contract plot. The Verwey transition point around 120 K is represented by a red triangle in (c).

**Figure S7.** Thermal rock magnetic cycling (TRMC) results for GA 84.6v. Hysteresis loops (top row), DCD curves (second row) and Day plots (third row) from room temperature to various target temperatures (100 °C, 200 °C, 300 °C, 400 °C, 450 °C, 500 °C, 550 °C and 575 °C and a repeated 575 °C measurement) made every 25 °C. After each heating step, samples were cooled to room temperature, during which no data was collected. The TRMC experiment includes nine heating-cooling cycles and measures over 100 sets of hysteresis loops and DCD curves. The duration of the whole measurement exceeds 300 hr. Differential DCD curves (remanent coercivity spectra) for the nine heating-cooling cycles are shown in the last row.

**Figure S8.** Low-field susceptibility curves for specimens GA 84.6v (a) and HS 2–8C (b) were obtained from the hysteresis loops during the TRMC experiment. The *Y*-axes represent low-field susceptibility measured at room temperature after each heating-cooling cycle. Each susceptibility value is normalized to the initial value before heating treatments. The *X*-axes represent the target temperatures of the TRMC method.

**Figure S9.** Magnetic coercivity distribution of GA 84.6v during the TRMC experiment. The grey circles were coercivity distribution data, and the orange curve shows the model fit results. The blue and purple curves represent the decomposed two coercivity components of the measured specimen. The blue curves displayed the low-coercivity component (LC), and the purple curves displayed the high-coercivity component (HC). The above magnetic constitute unmixed by DCD curves using the skew-normal distribution model of the MAX UnMix web application (Maxbauer *et al.* 2016).

**Figure S10.** Magnetic coercivity distribution of GA 84.6v during the TRMC experiment. The above magnetic constitute unmixed by DCD curves using the cumulative log Gaussian distribution model (Robertson & France 1994; Heslop *et al.* 2002). The red circles were coercivity distribution data, and the black curves show the model fit results. The red (LC) and oange (HC) curves represent the decomposed two coercivity components of the measured specimen.

**Figure S11.** FORC diagrams for specimen GA 84.6v at elevated temperatures during the TRMC experiment. The software package FORCinel v3.06 (Harrison & Feinberg 2008) was used to calculate the FORCs (field increment of 2 mT, 201 FORCs) with a SF of 4.

**Figure S12.** Thermal rock magnetic cycling (TRMC) results for the specimen HS 2–8C. We measured hysteresis loops (a) and DCD curves (b) at elevated temperatures from room temperature to each target temperature ( $100 \,^{\circ}\text{C}$ ,  $200 \,^{\circ}\text{C}$ ,  $300 \,^{\circ}\text{C}$ ,  $400 \,^{\circ}\text{C}$ ,  $500 \,^{\circ}\text{C}$ ,  $600 \,^{\circ}\text{C}$  and repeated  $600 \,^{\circ}\text{C}$ ) for every  $50 \,^{\circ}\text{C}$ . Then, cool it to room

temperature and do not collect any data. The TRMC experiment includes seven heating-cooling cycles, and the duration of the whole measurement is decreased to 80 hr.

**Figure S13.** Hysteresis parameters ( $B_c$ ,  $B_{cr}$ ) for specimen HS 2–8C at elevated temperatures from the TRMC experiment. The *Y*-axes represent  $B_c$  (a) and  $B_{cr}$  (b) values, respectively. The *X*-axes represent target temperatures ranging from 100 to 600 °C, including seven heating-cooling cycles. The measurements were conducted from room temperature to 600 °C in the seventh cycle (last cycle), then the specimen was cooled back to room temperature to complete the TRMC experiment, during which no measurements were made.

**Figure S14.** FORC diagrams for specimen HS 2–8C at elevated temperatures during the TRMC experiment. FORC diagrams measured at the same temperature are displayed in the same column, ranging from room temperature to 200 °C. The software package FORCinel v3.06 (Harrison & Feinberg 2008) was used to calculate the FORCs (field increment of 2 mT, 101 FORCs) with a SF of 4.

**Figure S15.** FORC diagrams for specimen HS 2–8C at elevated temperatures during the TRMC experiment. The software package FORCinel v3.06 (Harrison & Feinberg 2008) was used to calculate the FORCs (field increment of 2 mT, 101 FORCs) with a SF of 4.

Figure S16. (a) The result of IZZI-modified protocols for a Hawaii glassy volcanic specimen hw 120a4 (4770  $\pm$  90 yr B.P.) [figures and captions are modified from fig. 4 of Cromwell et al. (2018)]. The orange and green lines represent the linear regression from room temperature to 450 °C and 450–580 °C temperature interval, respectively. (b) Arai diagram with two linear segments for LT 21-5-1 from the Pliocene lava sequence in Iceland. The orange and green lines represent the linear regression from room temperature to 500 °C interval and 500-580 °C temperature interval, respectively [figures and captions are modified from fig. 6 of Tanaka & Yamamato (2016)]. (c) IZZI Thellier results for EH 22-13A from a late-Quaternary El Golfo section (EL Hierro) vield two palaeointensity estimates (39.4  $\mu$ T from the lower-temperature segment and 11.2  $\mu$ T from the high-temperature segment), and both pass the sets of selection criteria [figures and captions are modified from fig. 5 of Monster et al. (2018)].

**Table S1.** EPMA results of iron oxide minerals in specimen GA 84.6u (the first table). The major component is high-titanium titanomagnetite (Fe<sub>3-x</sub>Ti<sub>x</sub>O<sub>4</sub>), with a Ti content below 0.6. Nearly pure magnetite with  $x\sim0.06$  formed from deuteric oxidation and occurs as micron-scale particles in the measured specimen. EPMA results of iron oxide minerals in the after-heating specimen GA 84.6w (the second table). The major component is high-titanium titanomagnetite (Fe<sub>3-x</sub>Ti<sub>x</sub>O<sub>4</sub>), with a Ti content below 0.6. Nearly pure magnetite formed from deuteric oxidation occurs as submicronto micron-scale particles. The magnetic mineral composition and particle size distribution of the GA 84.6w at an after-heated state is similar to that of specimen GA 84.6u, indicating that thermophysical alteration of the measured specimen cannot be detected by EPMA analysis.

**Table S2.** Hysteresis parameters ( $M_{\rm s}$ ,  $M_{\rm rs}$ ,  $B_{\rm c}$ ,  $B_{\rm cr}$ ) for specimen GA 84.6v measured at elevated temperatures during low-temperature thermal fluctuation tomography (LT-TFT).  $M_{\rm s}$ ,  $M_{\rm rs}$  and  $B_{\rm c}$  were determined from high-field slope-corrected hysteresis loops, and  $B_{\rm cr}$  was extracted from DCD curves.

**Table S3.** Hysteresis parameters  $(M_s, M_{rs}, B_c, B_{cr})$  for Galapagos lava specimen GA 84.6v were measured at elevated temperatures during the TRMC experiment.  $M_s, M_{rs}$  and  $B_c$  were determined from high-field slope-corrected hysteresis loops, and  $B_{cr}$  was extracted from DCD curves.

**Table S4.** Hysteresis parameters  $(M_s, M_{rs}, B_c, B_{cr})$  for Mt Lassen specimen HS 2–8C were measured at elevated temperatures during the TRMC experiment.  $M_s, M_{rs}$  and  $B_c$  were determined from high-field slope-corrected hysteresis loops, and  $B_{cr}$  was extracted from DCD curves.

Please note: Oxford University Press are not responsible for the content or functionality of any supporting materials supplied by the authors. Any queries (other than missing material) should be directed to the corresponding author for the article.

#### CONFLICTS OF INTEREST

The authors declare no conflict of interest.

#### DATA AVAILABILITY

The raw rock magnetic data measured in this study can be downloaded at the figshare repository: https://doi.org/10.6084/m9.figshare.24580898.v3.

#### REFERENCES

- Abdulghafur, F. & Bowles, J.A., 2019. Absolute palaeointensity study of miocene Tiva Canyon Tuff, Yucca Mountain, 7 Nevada: role of fine-particle grain-size variations, *Geochem. Geophys. Geosyst.*, 20(12), 5818–5830.
- Asefaw, H., Tauxe, L., Koppers, A.A.P. & Staudigel, H., 2021. Four-dimensional paleomagnetic dataset: plio-pleistocene paleodirection and palaeointensity results from the Erebus Volcanic Province, Antarctica, J. geophys. Res., 126(2), 22.
- Balbas, A., Koppers, A.A.P., Kent, D.V., Konrad, K. & Clark, P.U., 2016.
  Identification of the short-lived Santa Rosa geomagnetic excursion in lavas on Floreana Island (Galapagos) by <sup>40</sup>Ar/<sup>39</sup>Ar geochronology, Geology, 44(5), 359–362.
- Biasi, J., Kirschvink, J.L. & Fu, R.R., 2021. Characterizing the geomagnetic field at high southern latitudes: evidence from the Antarctic Peninsula, J. geophys. Res., 126(12), 20.
- Biggin, A., 2006. First-order symmetry of weak-field partial thermore-manence in multi-domain (MD) ferromagnetic grains: 2. Implications for Thellier-type palaeointensity determination, *Earth planet. Sci. Lett.*, **245**(1-2), 454–470.
- Biggin, A.J., Piispa, E.J., Pesonen, L.J., Holme, R., Paterson, G.A., Veikkolainen, T. & Tauxe, L., 2015. Palaeomagnetic field intensity variations suggest mesoproterozoic inner-core nucleation, *Nature*, 526(7572), 245–248.
- Biggin, M.P. & Dekkers, M., 2007. A reliable absolute palaeointensity determination obtained from a non-ideal recorder, *Earth planet. Sci. Lett.*, 257(3-4), 545–563.
- Bono, R.K., Tarduno, J.A., Nimmo, F. & Cottrell, R.D., 2019. Young inner core inferred from Ediacaran ultra-low geomagnetic field intensity, *Nat. Geosci.*, 12(2), 143–147.
- Calvo-Rathert, M., Morales-Contreras, J., Carrancho, Á. & Goguitchaichvili, A., 2016. A comparison of Thellier-type and multispecimen palaeointensity determinations on pleistocene and historical lava flows from Lanzarote (Canary Islands, Spain), Geochem. Geophys. Geosyst., 17(9), 3638–3654.
- Calvo, M., Pr'evot, M., Perrin, M. & Riisager, J., 2002. Investigating the reasons for the failure of palaeointensity experiments: a study on historical lava flows from Mt. Etna (Italy), *Geophys. J. Int.*, 149(1), 44–63.
- Carvallo, C., Roberts, A.P., Leonhardt, R., Laj, C., Kissel, C., Perrin, M. & Camps, P., 2006. Increasing the efficiency of palaeointensity analyses by selection of samples using first-order reversal curve diagrams, *J. geophys. Res.*, 111(B12).

- Coe, R.S., 1967a. The determination of paleo-intensities of the Earth's magnetic field with emphasis on mechanisms that could cause non-ideal behaviour in Thellier's method, *J. Geomag. Geoelectr*, **19**, 157–179.
- Coe, R.S., 1967b. Paleo-intensities of the Earth's magnetic field determined from tertiary and quaternary rocks, J. geophys. Res., 72, 3247–3262.
- Coe, R.S., Riisager, J., Plenier, G., Leonhardt, R. & Krása, D., 2004. Multidomain behaviour during Thellier palaeointensity experiments: results from the 1915 Mt. Lassen flow, *Phys. Earth planet. Inter.*, 147(2-3), 141–153
- Cromwell, G., Tauxe, L., Staudigel, H. & Ron, H., 2015. Palaeointensity estimates from historic and modern Hawaiian lava flows using glassy basalt as a primary source material, *Phys. Earth planet. Inter.*, **241**, 44–56
- Cromwell, G., Trusdell, F., Tauxe, L., Staudigel, H. & Ron, H., 2018.
  Holocene palaeointensity of the Island of Hawai 'i from glassy volcanics,
  Geochem. Geophys. Geosyst., 19(9), 3224–3245.
- de Groot, L.V. et al., 2015. High palaeointensities for the Canary Islands constrain the Levant geomagnetic high, Earth planet. Sci. Lett., 419, 154–167.
- de Groot, L.V., Fabian, K., Bakelaar, I.A. & Dekkers, M.J., 2014. Magnetic force microscopy reveals meta-stable magnetic domain states that prevent reliable absolute palaeointensity experiments, *Nat. Commun.*, 5, 10.
- de Groot, L.V., Mullender, T.A.T. & Dekkers, M.J., 2013. An evaluation of the influence of the experimental cooling rate along with other thermomagnetic effects to explain anomalously low palaeointensities obtained for historic lavas of Mt Etna (Italy), Geophys. J. Int., 193(3), 1198–1215.
- Dekkers, M.J. & Böhnel, H.N., 2006. Reliable absolute palaeointensities independent of magnetic domain state, *Earth planet. Sci. Lett.*, 248(1-2), 508–517.
- Dunlop, D.J., 2002. Theory and application of the day plot (M<sub>rs</sub>/M<sub>s</sub> versus H<sub>cr</sub>/H<sub>c</sub>) 1. Theoretical curves and tests using titanomagnetite data, *J. geophys. Res.*, **107**(B3), 22.
- Dunlop, D.J., 2011. Physical basis of the Thellier-Thellier and related paleointensity methods, *Phys. Earth planet. Inter.*, 187(3-4), 118–138.
- Fabian, K., 2009. Thermochemical remanence acquisition in single-domain particle ensembles: a case for possible overestimation of the geomagnetic palaeointensity, *Geochem. Geophys. Geosyst.*, 10(6).
- Fu, R.R. et al., 2014. Solar nebula magnetic fields recorded in the Semarkona meteorite, Science, 346(6213), 1089–1092.
- Fu, R.R., Kehayias, P., Weiss, B.P., Schrader, D.L., Bai, X.N. & Simon, J.B., 2020. Weak magnetic fields in the outer solar nebula recorded in CR chondrites, *J. geophys. Res.*, 125(5).
- Grappone, J.M., Biggin, A.J. & Hill, M.J., 2019. Solving the mystery of the 1960 Hawaiian lava flow: implications for estimating Earth's magnetic field, *Geophys. J. Int.*, 218(3), 1796–1806.
- Grappone, J.M., Russell, J.M. & Biggin, A.J., 2021. Investigating the utility of a high-temperature Thellier-style palaeointensity experimental protocol, *Earth, Planets Space*, 73(1).
- Halls, H.C., McArdle, N.J., Gratton, M.N., Hill, M.J. & Shaw, J., 2004. Microwave palaeointensities from dyke chilled margins: a way to obtain long-term variations in geodynamo intensity for the last three billion years, *Phys. Earth planet. Inter.*, 147(2-3), 183–195.
- Harrison, R.J. & Feinberg, J.M., 2008. FORCinel: an improved algorithm for calculating first-order reversal curve distributions using locally weighted regression smoothing, *Geochem. Geophys. Geosyst.*, 9, 11.
- Herrero-Bervera, E. & Valet, J.-P., 2009. Testing determinations of absolute palaeointensity from the 1955 and 1960 Hawaiian flows, *Earth planet. Sci. Lett.*, **287**(3-4), 420–433.
- Heslop, D., Dekkers, M.J., Kruiver, P.P. & Oorschot, I.H.M.V., 2002. Analysis of isothermal remanent magnetization acquisition curves using the expectation—maximization algorithm, *Geophys. J. Int.*, 148(1), 58–64.
- Hoffman, K.A., Constantine, V.L. & Morse, D.L., 1989. Determination of absolute palaeointensity using a multi-specimen procedure, *Nature*, 339(6222), 295–297.
- Jackson, M., Carter-Stiglitz, B., Egli, R. & Solheid, P., 2006. Characterizing the superparamagnetic grain distribution f(V,Hk) by thermal fluctuation tomography, *J. geophys. Res.*, 111(B12).

- Jeong, D., Liu, Q., Yamamoto, Y., Yu, Y., Zhao, X. & Qin, H., 2021. New criteria for selecting reliable Thellier-type palaeointensity results from the 1960 Kilauea lava flows, Hawaii, Earth, Planets Space, 73(1), 10.
- Kent, D.V., Wang, H. & Rochette, P., 2010. Equatorial paleosecular variation of the geomagnetic field from 0 to 3 Ma lavas from the Galapagos Islands, *Phys. Earth Planet. Inter.*, **183**, 404–412.
- Kim, W., Doh, S.-J. & Yu, Y., 2018. Reliable palaeointensity determinations from late cretaceous volcanic rocks in Korea with constraint of thermochemical alteration, *Phys. Earth planet. Inter.*, 279, 47–56.
- Kosterov, A.A. & Pre'vot, M., 1998. Possible mechanisms causing failure of Thellier palaeointensity experiments in some basalts, *Geophys. J. Int.*, 134(2), 554–572.
- Lawrence, K.P., Tauxe, L., Staudigel, H., Constable, C.G., Koppers, A., McIntosh, W. & Johnson, C.L., 2009. Paleomagnetic field properties at high southern latitude, *Geochem. Geophys. Geosyst.*, 10, 27.
- Levi, S., 1977. The effect of magnetite particle size on paleointensity determinations of the geomagnetic field, *Phys. Earth planet. Inter.*, **3**, 245–259.
- Maxbauer, D.P., Feinberg, J.M. & Fox, D.L., 2016. MAX UnMix: a web application for unmixing magnetic coercivity distributions, *Comput. Geosci.*, 95, 140–145.
- Michalk, D.M., Biggin, A.J., Knudsen, M.F., Böhnel, H.N., Nowaczyk, N.R., Ownby, S. & López-Martínez, M., 2010. Application of the multispecimen palaeointensity method to pleistocene lava flows from the Trans-Mexican Volcanic Belt, *Phys. Earth planet. Inter.*, 179(3-4), 139–156.
- Michalk, D.M., Muxworthy, A.R., Böhnel, H.N., Maclennan, J. & Nowaczyk, N., 2008. Evaluation of the multispecimen parallel differential pTRM method: a test on historical lavas from Iceland and Mexico, *Geophys. J. Int.*, 173(2), 409–420.
- Mighani, S., Wang, H., Shuster, D.L., Borlina, C.S., Nichols, C.I.O. & Weiss, B.P., 2020. The end of the lunar dynamo, *Sci. Adv.*, **6**(1), 8.
- Monster, M.W.L., van Galen, J., Kuiper, K.F., Dekkers, M.J. & de Groot, L.V., 2018. A late-quaternary full-vector geomagnetic record from El Golfo section, El Hierro, Canary Islands, *Geophys. J. Int.*, 215(3), 1701–1717.
- Okayama, K., Mochizuki, N., Wada, Y. & Otofuji, Y.-i., 2019. Low absolute palaeointensity during late Miocene Noma excursion of the Earth's magnetic field, *Phys. Earth planet. Inter.*, 287, 10–20.
- Paterson, G.A., 2011. A simple test for the presence of multidomain behaviour during palaeointensity experiments, J. geophys. Res., 116, 12.
- Paterson, G.A., Muxworthy, A.R., Yamamoto, Y. & Pan, Y., 2017. Bulk magnetic domain stability controls palaeointensity fidelity, *Proc. Natl. Acad. Sci. U.S.A.*, 114(50), 13 120–13 125.
- Pike, C.R., Roberts, A.P. & Verosub, K.L., 1999. Characterizing interactions in fine magnetic particle systems using first order reversal curves, *J. appl. Phys.*, 85(9), 6660–6667.
- Qin, H., He, H., Liu, Q. & Cai, S., 2011. Palaeointensity just at the onset of the cretaceous normal superchron, *Phys. Earth planet. Inter.*, **187**(3-4), 199–211.
- Riisager, P. & Riisager, J., 2001. Detecting multidomain magnetic grains in Thellier palaeointensity experiments, *Phys. Earth planet. Inter.*, **125**(1-4), 111–117.
- Roberts, A.P., Heslop, D., Zhao, X. & Pike, C.R., 2014. Understanding fine magnetic particle systems through use of first-order reversal curve diagrams, *Rev. Geophys.*, 52(4), 557–602.
- Robertson, D.J. & France, D.E., 1994. Discrimination of remanence-carrying minerals in mixtures, using isothermal remanent magnetization acquisition curves, *Phys. Earth planet. Inter.*, **82**(3-4), 223–234.
- Rochette, P., Ben Atig, F., Collombat, H., Vandamme, D. & Vlag, P., 1997.
  Low paleosecular variation at the equator: a paleomagnetic pilgrimage from Galapagos to Esterel with Allan Cox and Hans Zijderveld, *Geologie en Mijnbouw*, 76, 9–19.
- Schmidt, P.W., 1993. Paleomagnetic cleaning strategies, *Phys. Earth planet. Inter.*, 76(1-2), 169–178.
- Shaar, R., Ron, H., Tauxe, L., Kessel, R. & Agnon, A., 2011. Paleomagnetic field intensity derived from non-SD: testing the Thellier IZZI technique on MD slag and a new bootstrap procedure, *Earth planet. Sci. Lett.*, 310(3-4), 213–224.

- Smirnov, A.V. & Evans, D.A.D., 2015. Geomagnetic palaeointensity at ~2.41 Ga as recorded by the Widgiemooltha Dike Swarm, Western Australia, *Earth planet. Sci. Lett.*, 416, 35–45.
- Smirnov, A.V. & Tarduno, J.A., 2003. Magnetic hysteresis monitoring of cretaceous submarine basaltic glass during Thellier palaeointensity experiments: evidence for alteration and attendant low field bias, *Earth planet. Sci. Lett.*, 206(3-4), 571–585.
- Smirnov, A.V., 2005. Thermochemical remanent magnetization in precambrian rocks: are we sure the geomagnetic field was weak?, *J. geophys. Res.*, 110(B6), 12.
- Smirnov, A.V., Kulakov, E.V., Foucher, M.S. & Bristol, K.E., 2017. Intrinsic palaeointensity bias and the long-term history of the geodynamo, *Sci.* Adv. 3(2), 7
- Tanaka, H. & Yamamoto, Y., 2016. Palaeointensities from pliocene lava sequences in Iceland: emphasis on the problem of Arai plot with two linear segments, *Geophys. J. Int.*, 205(2), 694–714.
- Tauxe, L. & Staudigel, H., 2004. Strength of the geomagnetic field in the cretaceous Normal Superchron: new data from submarine basaltic glass of the Troodos Ophiolite, Geochem. Geophys. Geosyst., 5, 16.
- Tauxe, L., Asefaw, H., Behar, N., Koppers, A.A.P. & Shaar, R., 2022.Palaeointensity estimates from the pleistocene of Northern Israel: implications for hemispheric asymmetry in the time-averaged field, *Geochem. Geophys. Geosyst.*, 23(9), 20.
- Tauxe, L., Santos, C.N., Cych, B., Zhao, X., Roberts, A.P., Nagy, L. & Williams, W., 2021. Understanding nonideal palaeointensity recording in igneous rocks: insights from aging experiments on lava samples and the causes and consequences of "fragile" curvature in Arai plots, Geochem. Geophys. Geosyst., 22(1), 24.
- Thellier, É. & Thellier, O., 1959. Sur l'intensité du champ magnétique terrestre dans le passé historique et géologique, *Ann. Geophys.*, **15**, 285–376.

- Thellier, É., 1977. Early research on the intensity of the ancient geomagnetic field, *Phys. Earth planet. Inter.*, **13**, 241–244.
- Tikoo, S.M., Weiss, B.P., Shuster, D.L., Suavet, C., Wang, H. & Grove, T.L., 2017. A two-billion-year history for the lunar dynamo, Sci. Adv., 3(8), 9.
- Valet, J.P., 2003. Time variations in geomagnetic intensity, *Rev. Geophys.*, 41(1), 44.
- Wang, H. & Kent, D.V., 2013. A palaeointensity technique for multidomain igneous rocks, Geochem. Geophys. Geosyst., 14(10), 4195–4213.
- Wang, H. & Kent, D.V., 2021. RESET: a method to monitor thermoremanent alteration in Thellier-Series palaeointensity experiments, *Geophys. Res. Lett.*, 48(5), 10.
- Wang, H. et al. 2017. Lifetime of the solar nebula constrained by meteorite paleomagnetism, *Science*, **355**(6325), 623–627.
- Wang, H., Kent, D.V. & Rochette, P., 2015. Weaker axially dipolar timeaveraged paleomagnetic field based on multidomain-corrected palaeointensities from Galapagos lavas, *Proc. Natl. Acad. Sci. U.S.A.*, 112(49), 15 036–15 041.
- Weiss, B.P., Bai, X.N. & Fu, R.R., 2021. History of the solar nebula from meteorite paleomagnetism, Sci. Adv., 7(1), 19.
- Xu, S. & Dunlop, D.J., 2004. Thellier palaeointensity theory and experiments for multidomain grains, *J. geophys. Res.*, **109**(B7), 13.
- Yamamoto, Y., Tsunakawa, H. & Shibuya, H., 2003. Palaeointensity study of the Hawaiian 1960 lava: implications for possible causes of erroneously high intensities, *Geophys. J. Int.*, 153(1), 263–276.
- Yu, Y., Tauxe, L. & Genevey, A., 2004. Toward an optimal geomagnetic field intensity determination technique, *Geochem. Geophys. Geosyst.*, 5, 24.
- Zhao, X., Liu, Q., Paterson, G.A., Qin, H., Cai, S., Yu, Y. & Zhu, R., 2014.
  The effects of secondary mineral formation on Coe-type palaeointensity determinations: theory and simulation, *Geochem. Geophys. Geosyst.*, 15(4), 1215–1234.